New metrics reveal the evolutionary continuum behind the morphological diversity of subglacial bedforms

Jean Vérité, Édouard Ravier, Olivier Bourgeois, Paul Bessin, Stéphane Pochat

New metrics reveal the evolutionary continuum behind the morphological diversity of subglacial bedforms

Article *in* Geomorphology · February 2023

DOI: 10.1016/j.geomorph.2023.108627

CITATION
1

READS
513

5 authors, including:

Jean Vérité
Institut de Physique du Globe de Paris
22 PUBLICATIONS **46** CITATIONS
SEE PROFILE

Edouard Ravier
Le Mans Université
52 PUBLICATIONS **393** CITATIONS
SEE PROFILE

Olivier Bourgeois
University of Nantes
189 PUBLICATIONS **2,380** CITATIONS
SEE PROFILE

Paul Bessin
Université du Maine
40 PUBLICATIONS **332** CITATIONS
SEE PROFILE

New metrics reveal the evolutionary continuum behind the morphological diversity of subglacial bedforms

Jean Vérité[1], Édouard Ravier[1], Olivier Bourgeois[2], Paul Bessin[1], Stéphane Pochat[2]

[1] *Laboratoire de Planétologie et Géosciences, UMR 6112, CNRS, Le Mans Université, Avenue Olivier Messiaen, 72085 Le Mans CEDEX 9, France*
[2] *Laboratoire de Planétologie et Géosciences, UMR 6112, CNRS, Nantes Université, 2 rue de la Houssinière, BP 92208, 44322 Nantes CEDEX 3, France*

Corresponding author: Jean Vérité (jean.verite@univ-lemans.fr)

Keywords: Glacial geomorphology; ribbed bedforms; drumlins; MSGLs; continuum; sinuous forms

Abstract

Understanding the formation of subglacial bedforms is primordial to constrain ice-meltwater-bed interactions and the dynamics of past and present ice sheets. However, the difficulty to observe active subglacial bedforms below present-day ice sheets implies that their formation and evolution are essentially deduced from the inversion of morphological and sedimentological data from palaeo-subglacial bedforms. In this study, the morphological characteristics of subglacial bedforms are explored with a new approach based on the combination of three dimensionless morphometric indices i.e., circularity index, sinuosity index and elongation component ratio. We measure the spatial distribution of these indices on an unpublished database composed of ~13,500 digitized bedforms taken from two selected portions of the Irish Ice Sheet and Laurentide Ice Sheet beds considering that (1) all subglacial bedforms in each region were formed under a single ice flow configuration and (2) the bedforms may have developed either orthogonal, parallel, or oblique to ice displacement directions. Our results reveal a morphometric and spatial continuum along which ribbed bedforms of various lengths and shapes – ranging from circular to elongated flow-transverse forms – are incipient bedforms that can evolve into transitional sinuous ribbed bedforms, then into predominantly flow-parallel sinuous bedforms that progressively realign to form streamlined bedforms. Assuming the glaciological contexts of selected study areas, this continuum may provide a new geomorphic criterion to constrain spatial variations in subglacial conditions (e.g. ice flow velocity, bedrock characteristics, meltwater pressure).

1. Introduction

Glacial geomorphologists have historically classified subglacial bedforms in different classes, based on their differences in shapes, dimensions and orientations in relation to a presupposed direction of ice flow (i.e. ice displacement direction). Linear ridges supposedly parallel to the ice flow direction have been called streamlined bedforms and include drumlins (***Hill, 1973; Menzies, 1979***), flutes (***Shaw et al., 2000; Eyles, 2012***), and mega-scale glacial lineations (MSGLs; ***Clark, 1993; Canals et al., 2000***) by order of increasing elongation ratios. Periodic ridges supposedly orthogonal to the ice flow direction have been defined as ribbed bedforms (***Stokes et al., 2016; Vérité et al., 2021***), and include bedforms that have been variously called ribbed moraines (***Cowan, 1968; Hättestrand, 1997***), Rogen moraines (***Lundqvist, 1969; Shaw, 1979***) and mega-ribs (***Greenwood and Kleman, 2010***) depending on their sizes and locations of first description. Sub-circular mounds without a determinable orientation have been referred to as circular bedforms (***Knight et al., 1999; Greenwood & Clark, 2008***), mammillary hills (***Aario, 1977***), ovoid forms (***Smith & Wise, 2007***) or hummocky ribbed bedforms (***Hättestrand, 1997; Dunlop & Clark, 2006; Möller & Dowling, 2015***). While parallelism between streamlined bedforms and ice flow directions has been confirmed below modern ice sheets and in front of retreating ice lobes (e.g. ***King et al., 2007; Johnson et al., 2010***), the relationship between orientation of other bedform classes and ice flow directions has not been proven.

Although these different morphological classes have sometimes been attributed to different subglacial formation processes, the alternative hypothesis that they may be part of a same morphometric, and perhaps genetic, continuum has emerged from the observation of spatial and morphometric transitions between ribbed and streamlined bedforms (**Fig. 1**) (***Carl, 1978; Aylsworth & Shilts, 1989; Dyke et al., 1992; Knight et al., 1999; Fannon et al., 2017***), between circular and ribbed bedforms (***Hättestrand, 1997; Dunlop and Clark, 2006; Greenwood & Clark, 2008; Vérité et al., 2022***), between different types of streamlined bedforms (e.g. ***Rose, 1987; Clark et al., 2009; Stokes et al., 2013; Sookhan et al., 2021, 2022***), and between circular, ribbed and streamlined bedforms *(**Aario, 1977; Markgren & Lassila, 1980; Ely et al., 2016**)*.

Several additional classes have also been proposed to describe more specific or more complex bedforms, such as smooth-sided/drumlinized ribbed moraines (**Fig. 1b**) (***Carl, 1978; Lundqvist, 1981;***

Dunlop & Clark, 2006), Blattnick moraines (**Fig. 1c**) (***Markgren & Lassila, 1980***), transverse/asymmetrical drumlins (**Fig. 1d**) (***Shaw, 1983; Boulton, 1987; Knight, 1997***), crescentic/parabolic ridges and drumlins (**Fig. 1e**) (***Boulton, 1987; Lundqvist, 1989; Smalley & Warburton, 1994; Maclachlan & Eyles, 2013; Eyles et al., 2016***), barchan-shaped (**Fig. 1f**), blocky angular (**Fig. 1g**) and jagged-type ribbed moraines (**Fig. 1h**) (***Dunlop & Clark, 2006***), extensional ribbed moraines (**Fig. 1i**) (***Wagner, 2014***), oblique ribbed bedforms (**Fig. 1j**) (***Vérité et al., 2021***) and channeled drumlins (**Fig. 1k**) (***Sookhan et al., 2021***) among others. Since most of these complex bedforms are sinuous, i.e. have a non-rectilinear crestline, and/or have apparently no clear orientation relative to the local ice flow direction, they do not fit with usual bedform classes and have therefore been excluded from most of the existing models of subglacial bedform continuum governed by ice flow direction and velocity (***Aario, 1977; Stokes et al., 2013***).

Complex bedforms have frequently been interpreted as resulting from the remolding of bedforms or the superimposition/crosscutting of several generations of bedforms such as drumlins and ribbed bedforms (***Rose & Letzer, 1975, 1977; Knight et al., 1999; Dunlop & Clark, 2006; Mitchell & Riley, 2006; De Angelis & Kleman, 2007; Greenwood & Clark, 2009***), in response to changes in ice flow direction (***Clark et al., 1993; Stokes et al., 2006a; Brown et al., 2011***) or/and velocity (***Stokes et al., 2006b, 2008***).

A demonstration that all subglacial bedform classes, including usual and complex ones, may or may not be part of a same spatial, morphometric and perhaps evolutionary continuum is missing. Previous attempts were based on two main preliminary assumptions: (1) elongated bedforms may be classified a-priori as either parallel or orthogonal to ice flow direction; (2) complex (oblique and/or sinuous) bedforms cannot form under constant ice flow directions. Without invoking changes in ice flow directions, physical modeling (**Fig. 1j**) (***Vérité et al., 2021***), glacial geomorphology (**Fig. 1k**) (***Sookhan et al., 2021***) and numerical modelling (***Ely et al., 2022***) recently demonstrated that complex bedforms, referred to as oblique ribbed bedforms, channeled drumlins and diagonal ribs, can develop under the same ice flow direction as transverse ribbed bedforms and streamlined bedforms respectively. Therefore, we perform here a systematic morphometric analysis of ~13,500 subglacial bedforms mapped in selected portions of the Irish and Laurentide Ice Sheet beds, only assuming that

streamlined bedforms develop parallel to the local ice flow direction. We quantify the complexity and variability of subglacial bedform shapes in these regions with three dimensionless morphometric indices and a spatial analysis of subglacial bedform distribution. We propose that all subglacial bedforms stand along an overall morphometric and spatial continuum that corresponds to an evolutionary continuum.

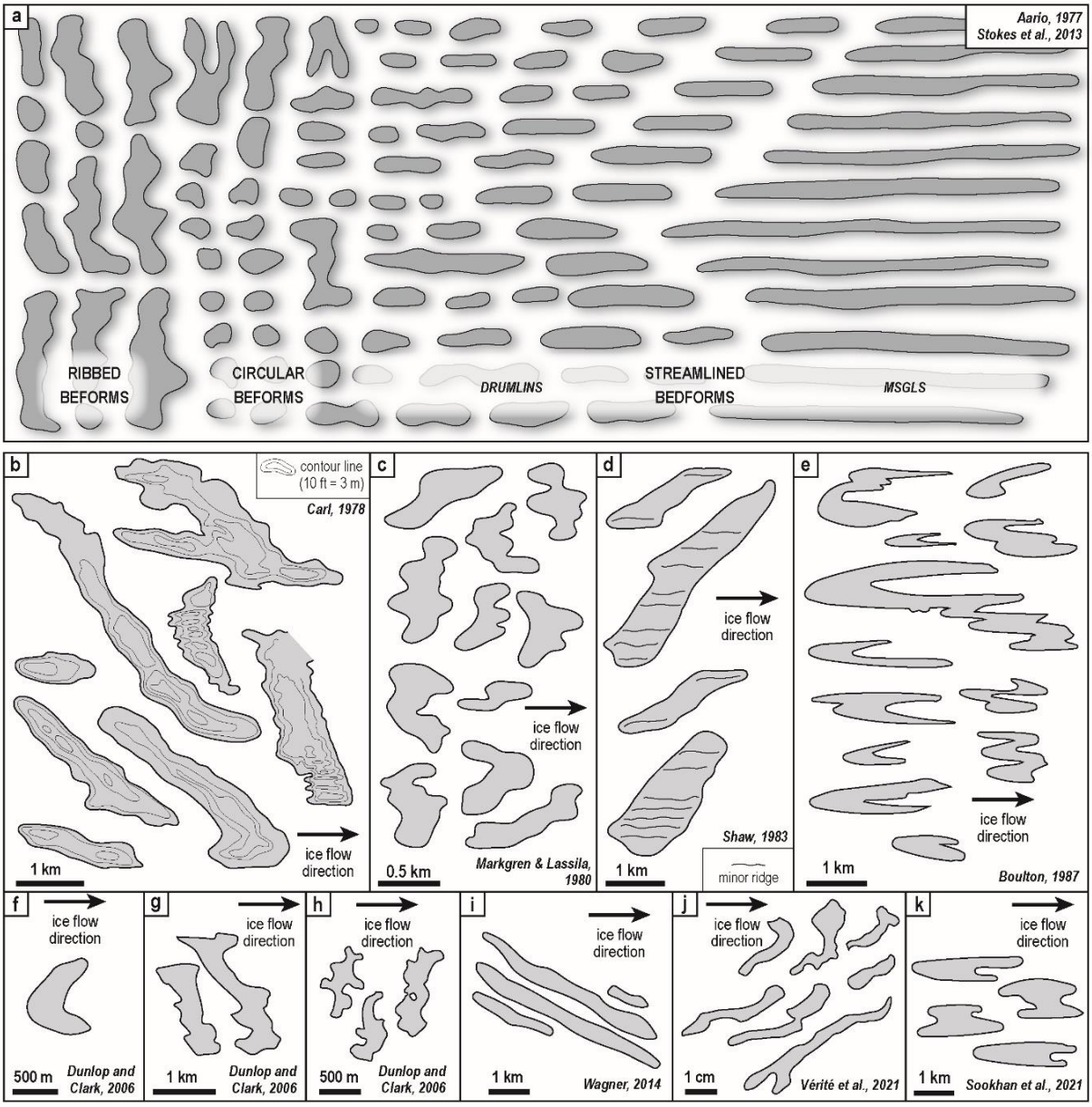

Figure 1. *(a) Schematic representation, as currently envisioned, of the subglacial bedform continuum between ribbed, circular and streamlined bedforms (drumlins and MSGLs) (after* ***Aario, 1977*** *and* ***Stokes et al., 2013****). (b) to (j) Examples of complex subglacial bedforms commonly associated with fields of ribbed and streamlined bedforms but excluded from the existing models of subglacial bedform continuum. They are referred to as (b) smoothsided/drumlinized ribbed moraines (****Carl, 1978****), (c) Blattnick moraines (****Markgren & Lassila, 1980****), (d) transverse/asymmetrical drumlins (****Shaw, 1983****), (e) parabolic drumlins (****Boulton, 1987*** *for mapping ;* ***Eyles et al., 2016*** *for denomination), (f) barchan-shaped, (g) blocky angular and (h) jagged-type ribbed moraines (****Dunlop & Clark, 2006****), (i) extensional ribbed moraines (****Wagner, 2014****), (j) oblique ribbed bedforms (****Vérité et al., 2021****) and (k) channeled drumlins (****Sookhan et al., 2021****).*

2. Data and method

2.1. Study areas

The two study areas are selected for (i) their great diversity of subglacial bedforms and (ii) the occurrence of complex forms at the spatial transitions between fields of ribbed and streamlined bedforms (**Fig. 2**). The first study area (11,300-km²) is located in northeastern Ireland, where a layer of subglacial till, commonly more than 15 m thick and deposited below the Irish Ice Sheet (IIS) during the last Devensian glaciation, covers the Paleozoic sedimentary bedrock (***McConnell & Gatley, 2006***). Large-scale streamlined bedform tracts that have been interpreted as corridors of fast ice flow (***Stokes & Clark, 1999; Greenwood & Clark, 2009a***) and possibly ice streams (***Synge & Stephens, 1960***) are reported south of the northern ice divide of the Lowland Ice Dome between 20 and 17 ka BP (***Clark et al., 2022***) and downstream from ribbed and circular bedform fields (***Dunlop & Clark, 2006; Greenwood & Clark, 2008***). Based on frequent apparent superimposition and crosscutting relationships between bedforms over the study area, the geomorphological record has been interpreted as a superimposition of several configuration of ice-sheet flow trajectories (***Greenwood & Clark, 2009a,b***).

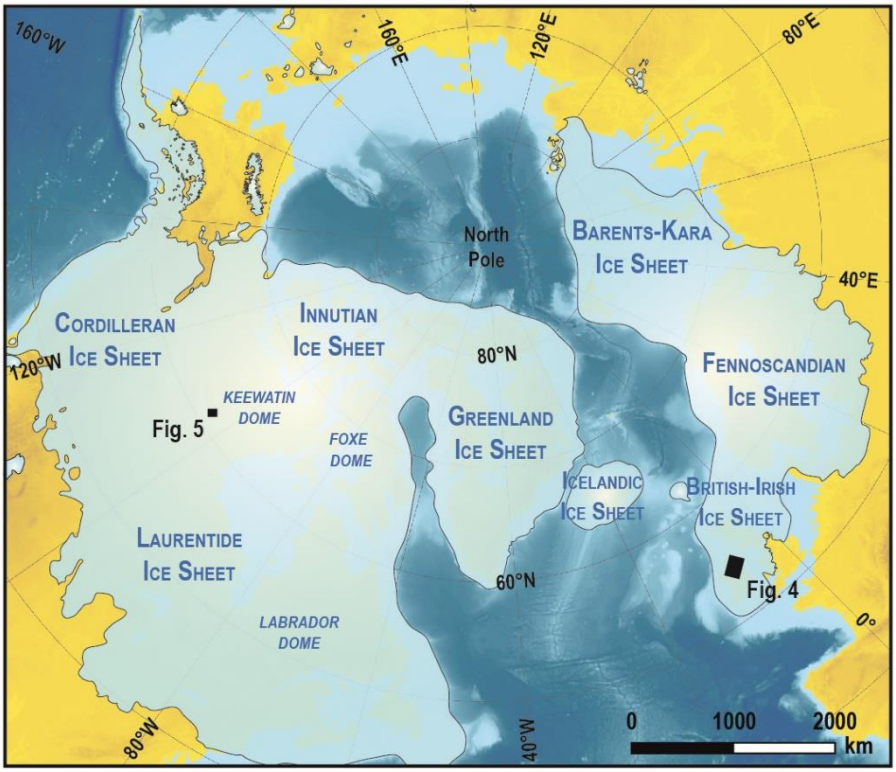

Figure 2. *Location of study areas relative to the maximum extension of the northern hemisphere ice sheets during the Last Glacial Maximum (**Batchelor et al., 2019**).*

The second study area (2,100-km²) is located west of the Hudson Bay in northern Canada, between Firedrake Lake and Boyd Lake (**Fig. 2**). The area was covered by the Keewatin Ice Dome of the Laurentide Ice Sheet (LIS) during the last Wisconsinian glaciation and the surficial geology is characterized by a 10 m thick (at most) layer of subglacial till deposited over a Precambrian bedrock (***Shilts et al., 1979***; ***Dyke et al., 1989***). Ribbed and streamlined bedform tracts laterally alternate, radiating outwards from the Keewatin ice divide (***Shilts et al., 1987; Aylsworth and Shilts, 1989***) and paralleling meltwater corridors described in the Keewatin area by ***Storrar et al. (2013)*** and ***Lewington et al., (2019, 2020).***

2.2. Data sources and processing

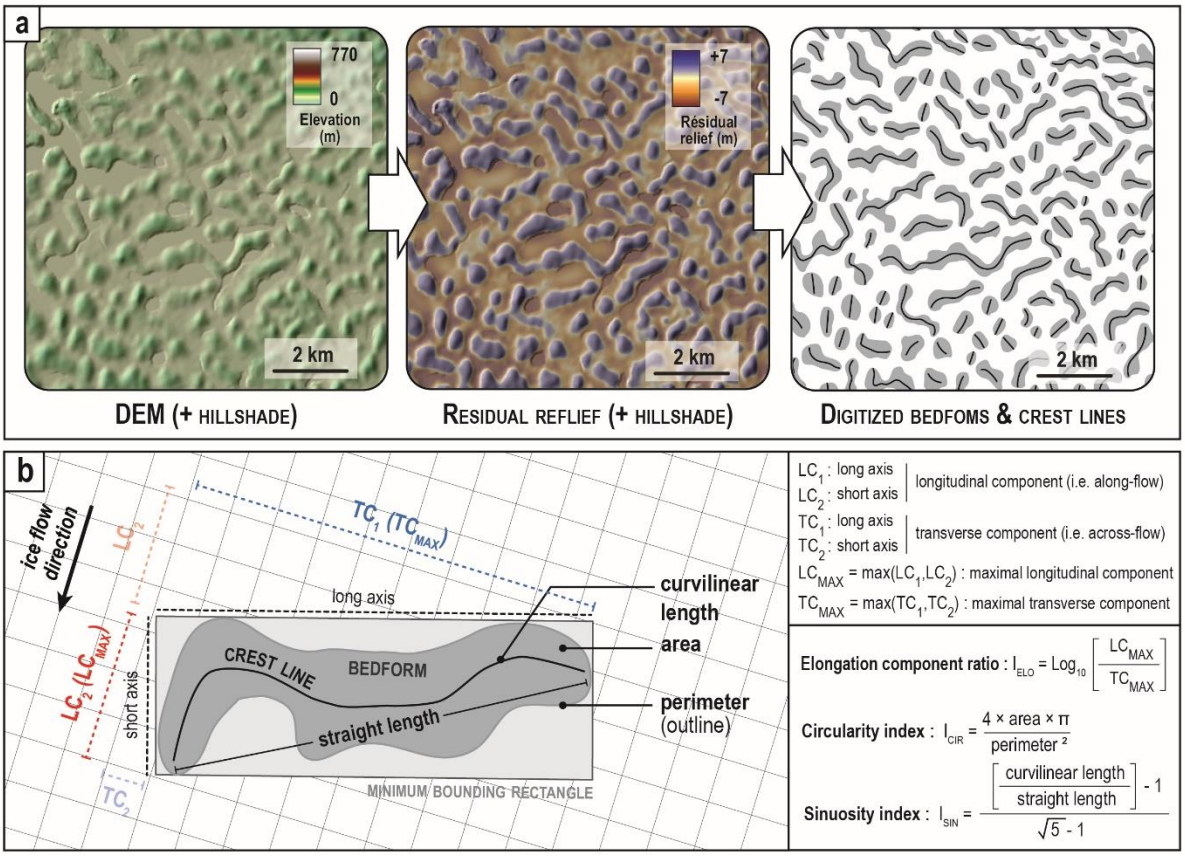

Figure 3*. (a) Hillshaded residual relief derived from a digital elevation model and from which bedform outlines and crest lines are manually digitized. (b) Measured quantities for the calculation of dimensionless indices: elongation component ratio (I_{ELO}), circularity index (I_{CIR}) and sinuosity index (I_{SIN}).*

We conduct subglacial bedform mapping from open-data DEMs of the LIS bed in Canada (10-m DEMs; ArcticDEM, https://www.pgc.umn.edu/data/arcticdem/, ***Porter et al., 2018***) and IIS bed in Ireland (25-m DEMs; EU-DEM v1.1, https://land.copernicus.eu/) ; the resolution of the DEMs is better than 30 m to minimize misrepresentation of subglacial bedform sizes and shapes (***Napieralski***

and Nalepa, 2010). From these DEMs, we derive and superimpose unidirectional hillshade maps and residual relief maps (***Hillier & Smith, 2008***) with a Geographic Information System (GIS) software (**Fig. 3a**). The 1-m contour lines of residual relief data are manually delineated to produce bedform outlines. Lines of maximum elevation, manually delineated within each outlined bedform, represent the bedform crest line (**Fig. 3a**). The manual digitization is performed by a single mapper in order to avoid bias related to mapping experience, with a graphic tablet and using a freehand drawing tool. The digitization is performed at a constant 1:10 000 scale to counteract differences in DEM resolutions for the two selected study areas. A last step of manual correction carried out from hillshaded DEMs by removing outlier features and adding bedforms smaller than the radius of residual relief, provide the final modifications to the dataset.

2.3. Morphometric analysis

2.3.1. Current morphometric techniques on subglacial bedforms

Subglacial bedform shapes are classically characterized by their dimensions, orientations relative to the supposed ice flow direction, and degrees of elongation. ***Hollingworth (1931)*** defined the 'length/width' ratio on drumlins, which has been later referred to as the 'elongation ratio' (e.g. ***Doornkamp and King, 1971; Mills, 1987; Rose, 1987***). Later, the elongation ratio was abundantly used to distinguish different types of streamlined bedforms such as flutes, drumlins, mega-flutes, mega-drumlins, lineations and MSGLs (***Boyce and Eyles, 1991; Knight, 1997; O Cofaigh et al., 2002; Stokes & Clark, 2002; Briner, 2007; Clark et al., 2009; Dowling et al., 2015***). The 'length/width' ratio has also been used to characterize the shape and dimensions of different sub-classes of ribbed bedforms, such as ribbed/Rogen moraines (***Dunlop & Clark, 2006***), mega-ribs (***Greenwood & Kleman, 2010***) and traction ribs (***Stokes et al., 2016***), for which, unlike drumlins, the length was measured perpendicular to the ice flow direction. In an attempt to integrate ribbed, circular and streamlined bedforms in a unique morphometric dataset, ***Ely et al. (2016)*** redefined the elongation ratio as the down-ice length of bedforms (i.e. the length of streamlined bedforms and the width of ribbed bedforms) divided by their across-ice length (i.e. conversely). Assuming that bedforms are

either orthogonal or parallel to ice displacement directions, the possibility that they may be oblique to ice displacement was ignored.

Using the equations provided by ***Folk (1968)*** and ***Moellering & Rayner (1979)*** who respectively studied the shapes of sedimentary grains and catchment areas, ***Burgess et al. (2003)*** computed three dimensionless shape indices (compactness, circularity, and shape factor) on subglacial bedforms from their perimeters and areas to study the complex and contorted shapes of hummocky and Rogen moraines in Canada. Recently, ***Vérité et al. (2022)*** calculated the sinuosity index of bedform crest lines to demonstrate a morphometric continuum between ribbed bedforms and murtoos, assuming that murtoos are the most sinuous subglacial bedforms. Compared with length, width and elongation ratio, dimensionless shape indices used by ***Burgess et al. (2003)*** and ***Vérité et al. (2022)*** (i.e. compactness, circularity, shape factor, sinuosity) describe the complexity of subglacial bedform outlines and crest lines but they do not allow to characterize their orientation with respect to ice flow.

2.3.2 Definition of morphometric indexes

Using the same method as ***Vérité et al. (2022)***, we measure the perimeters and areas of bedform outlines and the curvilinear and straight lengths of bedform crest lines (**Fig. 3b**). In order to characterize the complex shapes of bedform outlines and crestlines, we use these dimensioned shape indices to calculate their circularity (I_{CIR}) (**Table 1.A**) and sinuosity (I_{SIN}) (**Table 1.B**) respectively. The maximal height (h_{MAX}), defined as the amplitude, is also measured for each bedform.

We complement this morphometric protocol to describe the diversity of elongation and orientation of subglacial bedforms relative to the ice flow direction (**Fig. S1**). We assume that all bedforms were formed under constant ice flow fields, considering no cross-cutting relationships of streamlined bedforms are observed (discussed in Section 4.2). Using a method inspired from those developed by ***Ng & Hughes (2019)***, we use streamlined bedforms as proxies for reconstructing ice flow fields and local ice flow directions. To do so, we derive the average orientation of the long-axis of streamlined bedforms, sampled in a hexagonal grid, to build the resulting vectors of ice flow direction in each hexagonal grid and to attribute a local ice flow direction to each bedform located in the hexagonal grid. In areas where streamlined bedforms are absent, we extrapolate ice flow directions from adjacent areas, with a method based on the principle of nearest neighborhood (**Figs. 4-5**). Since the orientation

of the long-axis of streamlined bedforms varies spatially, the nearest neighborhood in a hexagonal grid is more convenient than in a rectangular grid (***Birch et al., 2007***). The hexagonal grid area is chosen to ensure the presence of a minimum of 10 subglacial bedforms in each cell.

To allow the possibility that bedforms can be oblique to ice flow directions and to quantify this obliquity, we develop a new morphometric index called "elongation component ratio", computed from transverse (i.e. across-flow) and longitudinal (i.e. along-flow) components for each bedform (**Fig 3b**). Using minimum bounding rectangles, we automatically measure the lengths of transverse and longitudinal components for the long axis (i.e. TC_1 and LC_1) and the short axis (i.e. TC_2 and LC_2) of each bedform (**Fig. 3b**). From the ratio between the maximal transverse (TC_{MAX}) and maximal longitudinal components (LC_{MAX}), we compute the "elongation component ratio" (I_{ELO}) (**Table 1.C**), which integrates both orientation and elongation of bedforms (**Fig. S2**).

Table 1. *Description of dimensionless morphometric indices.*

Shape indices	Formula	Signification	Range of values & typical values
(A) Circularity index (I_{CIR})	$I_{CIR} = \frac{4 \times A \times \pi}{P^2}$	Compares the perimeter (P) of a bedform outline of a given area (A) with the perimeter of a circle of an identical area (***Burgess et al., 2003***).	**I_{CIR} : [0 ; 1]** I_{CIR} = 0 : strongly non-circular outline I_{CIR} = 1 : perfectly circular outline
(B) Sinuosity index (I_{SIN})	$I_{SIN} = \frac{\frac{Curvilinear\ length}{Straight\ length} - 1}{\sqrt{5} - 1}$	Measures the sinuosity of the crest line (i.e. ratio between the curvilinear length of the crest line and its straight length; ***Schumm, 1963***), normalized to the sinuosity of an equilateral triangle[1] (***Vérité et al., 2022***).	**I_{SIN} : [0 ; +∞]** I_{SIN} = 0 : perfectly linear crest line I_{SIN} = 1 : equilateral triangular crest line $I_{SIN} \rightarrow +\infty$: strongly sinuous crest line
(C) Elongation component ratio (I_{ELO})	$I_{ELO} = \log_{10}(\frac{LC_{MAX}}{TC_{MAX}})$	Measures the ratio between the maximal longitudinal (i.e. along-flow; LC_{MAX}) and the maximal transverse (i.e. across-flow; TC_{MAX}) components of a bedform, expressed on a logarithmic scale.	**I_{ELO} : [-∞ ; +∞]** $I_{ELO} \rightarrow -\infty$: $TC_{MAX} >> LC_{MAX}$ elongated transverse to the flow direction I_{ELO} = 0 : $TC_{MAX} \sim LC_{MAX}$ elongated equally transverse and parallel to the flow direction $I_{ELO} \rightarrow +\infty$: $LC_{MAX} >> TC_{MAX}$ strongly elongated parallel to the flow direction

[1] These morphometric indices are defined so that they can be applied to all subglacial bedforms currently described, including hummocks and murtoos that are not mentioned in this study. The sinuosity ratio is here normalized to the sinuosity ratio of an equilateral triangle, corresponding to the ratio between the length of two sides and the length of one side. The shape of equilateral triangle typically corresponds to the shape of 'murtoos', considered as the most sinuous bedforms currently described in the glacial literature.

3. Results

3.1. A morphometric continuum of subglacial bedforms

The results of our morphometric measurements in northeastern Ireland (n = 10,100; **Fig. 4**) and in northern Canada (n = 3,400; **Fig. 5**) have been compiled in a single dataset. First, there is no cluster or gap but a continuum in the distribution of bedform morphometric values (**Fig. 6; Figs. S2, S3**). All analyzed bedforms stand along a continuum between four end members, which are schematically portrayed in red in **Fig. 6** and correspond to minimal and maximal values of the dimensionless morphometric indices presented in **Table 1**. The 1st end-member corresponds to linear bedforms transverse to the ice flow direction with a I_{SIN} close to 0 and a I_{ELO} approaching -∞. The 2nd end member corresponds to circular bedforms showing a I_{CIR} = 1, a I_{SIN} = 0 and a I_{ELO} = 0. The 3rd end member corresponds to linear bedforms parallel to the ice flow direction with a I_{SIN} close to 0 and a I_{ELO} approaching +∞. Finally, the 4th end member corresponds to bedforms displaying a highly sinuous shape (I_{SIN} close to 1) without any dominant elongation component (I_{ELO} = 0).

Between the 1st and 2nd end members lies a category corresponding to bedforms transverse to the ice flow direction ($0 > I_{ELO} > -\infty$), with a linear crest line ($I_{SIN} \sim 0$) and a slightly undulating outline: these bedforms are referred as linear ribbed bedforms since they share all characteristics defined by ***Dunlop and Clark (2006)***. Linear ribbed bedforms have a TC_{MAX} ranging from 600 to 1250 m, a LC_{MAX} ranging from 300 to 550 m and an amplitude h_{MAX} ranging from 9 to 19 m. By approaching the 2nd end member, linear ribbed bedforms become less elongated and more circular. These observations are consistent with the hypothesis of a morphometric continuity among linear ribbed bedforms, as suggested by ***Hättestrand (1997), Dunlop and Clark (2006), Möller and Dowling (2015)*** and ***Vérité et al. (2021, 2022)***.

Between the 2nd and 3rd end members lies a category corresponding to bedforms parallel to the ice flow direction ($0 < I_{ELO} < +\infty$) with an ovoid shape and a linear crest line ($I_{SIN} \sim 0$). Typically, these bedforms have a homogenous TC_{MAX} ranging from 200 to 400 m, and a LC_{MAX} ranging from 500 to 2000 m as they approach the 3rd end member. Their amplitudes h_{MAX} ranging from 4 to 14 m, decrease towards the 3rd end member. These bedforms are typically referred to as streamlined bedforms and

form a continuum between bedforms classically subdivided in drumlins and MSGLs depending if they are respectively low- or highly-elongated, as suggested by ***Stokes et al. (2013)*** and ***Ely et al. (2016)***.

Other bedforms, representing 44% of the morphometric cluster, are neither parallel nor transverse to the ice flow direction and have more sinuous crest lines than linear ribbed and streamlined bedforms (**Fig. 6**).

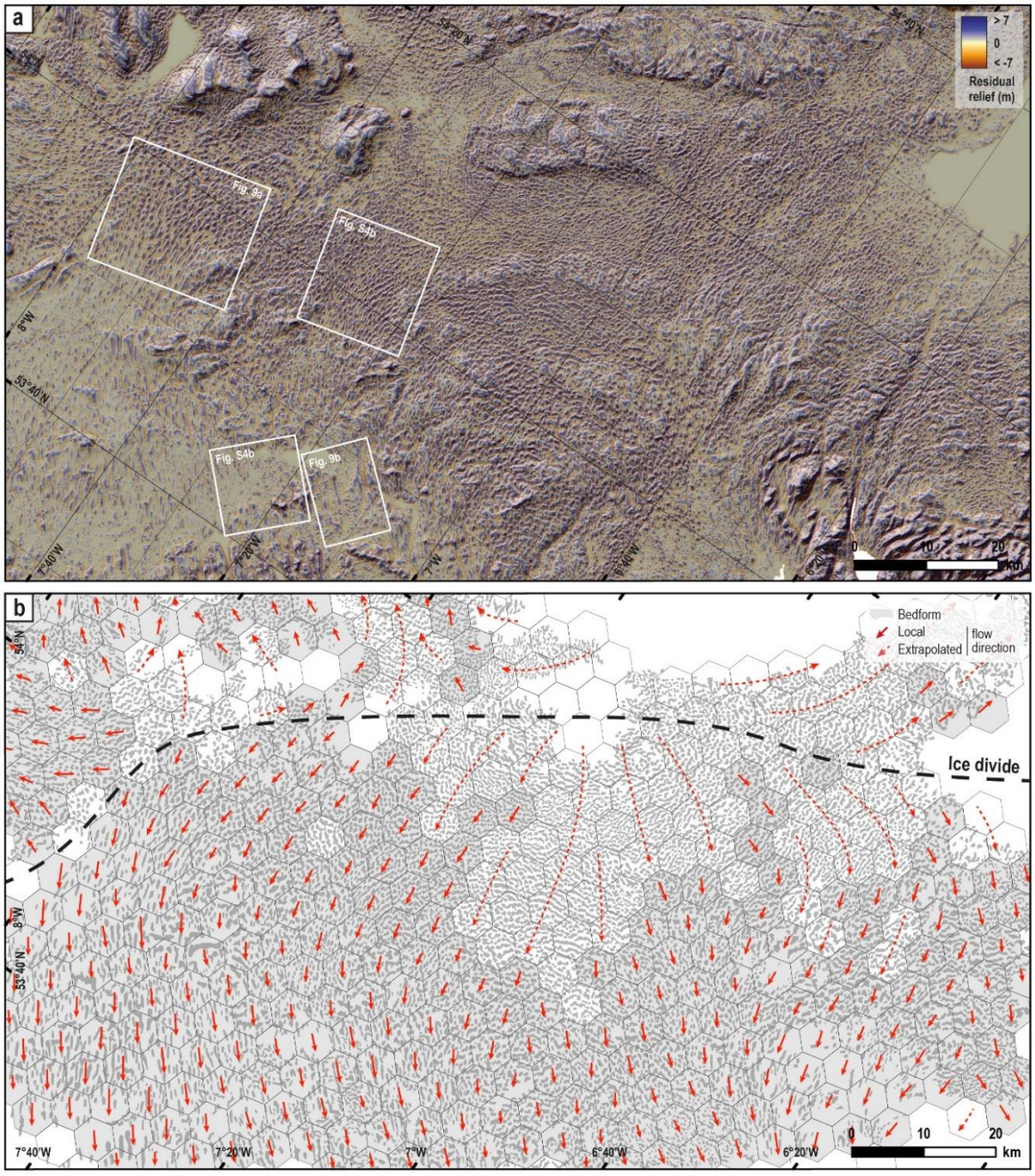

Figure 4. *(a) Hillshaded residual relief and (b) interpretative map with digitized bedforms of a portion of the Irish Ice Sheet bed in northeastern Ireland. Reconstruction of local ice flow directions (solid red lines) from sampled glacial lineations in a grid of 25-km² hexagons based on the assumption that the formation of streamlined bedforms is associated to a unique configuration of ice flow trajectories. Where streamlined bedforms are absent (white hexagons), the average flow direction is extrapolated (dotted red lines) from surrounding glacial lineations (grey hexagons). The ice divide (black stippled line) revealed by diverging flowsets is consistent with ice sheet reconstructions from* ***Greenwood and Clark (2009a,b)***.

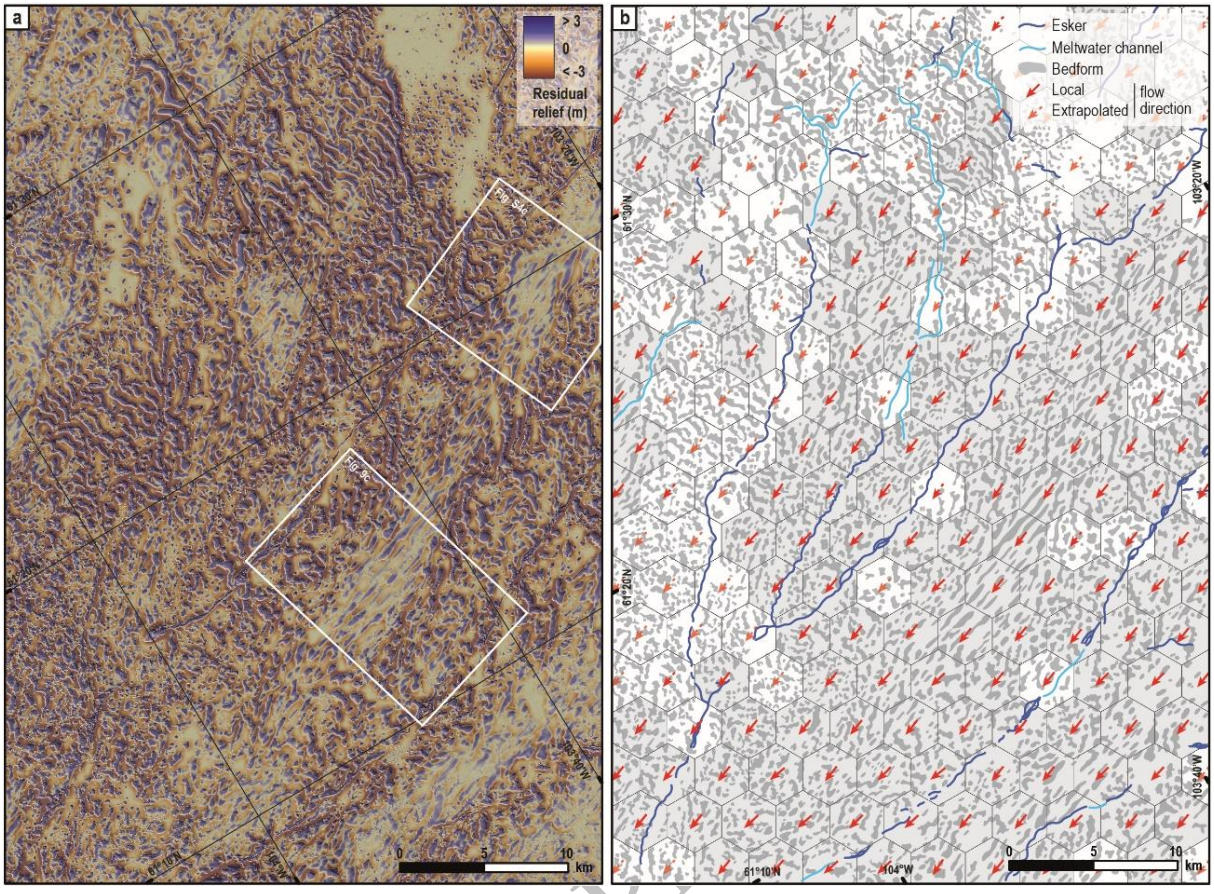

***Figure 5**. (a) Hillshaded residual relief and (b) interpretative map with digitized bedforms of a portion of the Laurentide Ice Sheet bed in northern Canada, between Firedrake Lake and Boyd Lake. Reconstruction of local ice flow directions in a grid of 9-km² hexagons with the same method as described in **Fig. 4**.*

Between the 1st and 4th end members, bedforms are sinuous (I_{SIN} > 0) and predominantly flow-transverse (I_{ELO} < 0). These bedforms are morphologically related to linear ribbed bedforms: they share a mainly transverse orientation relative to the ice flow direction (i.e. TC_{MAX} > LC_{MAX}) (**Fig. 6**) and have a similar TC_{MAX} ranging between 700 and 1400 m. However, they differ from linear ribbed bedforms by their higher LC_{MAX} ranging between 500 and 850 m, and their higher crest line sinuosity, typically ranging between 0.1 and 0.35. On average, their I_{SIN} is increasingly high as their I_{ELO} increases and tends to 0, and their I_{CIR} decreases as their I_{SIN} increases (**Fig. 6**). These bedforms are typically 9 to 20 m in amplitude. Examples of sinuous and predominantly flow-transverse bedforms have usually been reported as ribbed moraines although their sinuous appearance and their shape complexity have led some authors to create sub-categories of ribbed bedforms with new descriptive terms, such as Blattnick moraines (***Markgren and Lassila, 1980***), drumlinized/smooth-sided ribbed moraines (***Carl, 1978; Lundqvist, 1981; Dunlop and Clark, 2006***), blocky angular or jagged-type ribbed moraines (***Dunlop & Clark, 2006***) (**Fig. 1**). Considering their morphological similarities with

linear ribbed bedforms but also their higher degree of complexity, we refer to these sinuous and predominantly flow-transverse bedforms as sinuous ribbed bedforms.

Between the 3rd and 4th end members, when the LC_{MAX} exceeds the TC_{MAX}, bedforms are sinuous (I_{SIN} > 0) and predominantly parallel to the ice flow direction ($I_{ELO} \geq 0$). On average, their I_{SIN} decreases as their I_{ELO} increases and their I_{CIR} decreases as their I_{SIN} increases (**Fig. 6**). Their TC_{MAX} typically ranges between 350 and 750 m and is half of the linear and sinuous ribbed bedforms ones, while their LC_{MAX} typically ranging between 550 and 1200 m overlaps those of streamlined bedforms. These bedforms display lower amplitude than sinuous ribbed bedforms (h_{MAX} = 7–17 m). Although sinuous and predominantly flow-parallel bedforms are more similar to streamlined bedforms than ribbed bedforms, their TC_{MAX} are on average two times longer and their crest line sinuosity (I_{SIN} = 0.05–0.25 m) is much higher than those of streamlined bedforms.

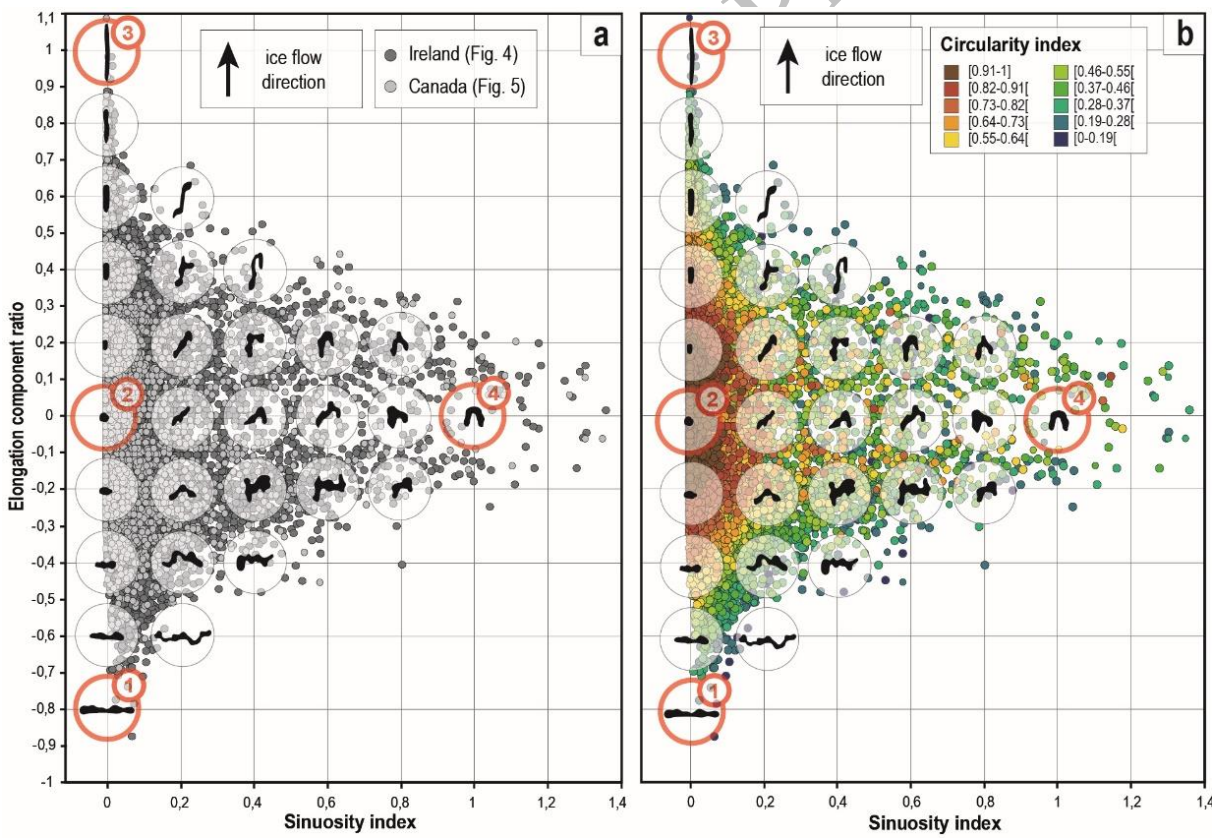

***Figure 6**. Plots of elongation component ratio (I_{ELO}) and sinuosity index (I_{SIN}). (a) Irish (dark grey dots) and Canadian bedforms (light grey dots). Selected bedform outlines picked up from the database are shown at each node of the grid to illustrate how I_{SIN} and I_{ELO} reflect their shapes. (b) Dot color refers to the circularity index (I_{CIR}) value of bedforms, reflecting its relation with both I_{ELO} and I_{SIN}. Both graphs highlight a morphometric continuum of bedforms in which four end members, corresponding to the minimal and maximal values of the dimensionless morphometric indices (I_{ELO}, I_{SIN} and I_{CIR}; see **Table 1**), are highlighted by red circles. Note that subglacial bedforms standing along the ordinate axis (I_{SIN} ~ 0) correspond to bedforms typically integrated in current models of bedform continuum, unrevealing a wider a morphometric continuum of bedforms.*

Some are highly sinuous with a U-shape, resembling bedforms referred to as crescentic/parabolic drumlins (***Boulton, 1987; Lundqvist, 1989; Smalley and Warburton, 1994; Maclachlan and Eyles, 2013; Eyles et al., 2016***), barchan-shaped ribbed moraines (***Dunlop and Clark, 2006***) or channeled drumlins (***Sookhan et al., 2021***) in the literature; while others are slightly sinuous, oblique to the flow direction and similar to bedforms described in the literature as oblique ribbed bedforms (***Vérité et al., 2021***), extensional ribbed moraines (***Wagner, 2014***), transverse/asymmetrical drumlins (***Shaw, 1983; Boulton, 1987***; ***Knight, 1997***) or drumlinized moraines (***Carl, 1978; Brown et al., 2011***) (**Fig. 1**).

3.2. Spatial distribution of subglacial bedform morphometrics

To investigate whether the morphometric continuum described in Section 3.1 is supported by a spatial continuum, we describe now the distribution of bedform shapes in the two study areas. To do so, we explore the evolution of bedform morphological indices at the transition between flow-perpendicular and flow-parallel bedforms, both at regional (**Figs. 7-8**) and local scales (**Figs. 9-10; Fig. S4**).

3.2.1. Ireland

In the northern part of the Irish study area, flow-perpendicular ($I_{ELO} < 0$) and linear ($I_{SIN} < 0.1$) bedforms, i.e. linear ribbed bedforms, gather in a 70-km long and 30-km wide field lying along the ice divide (**Figs. 7a-b**). To the south, flow-parallel ($I_{ELO} > 0$) and linear ($I_{SIN} < 0.1$) bedforms, i.e. streamlined bedforms, gather in a 60-km long and 40-km wide field (**Figs. 7a-b**). The progressive increase in I_{ELO} from north to south highlights that streamlined bedforms are increasingly elongated, ranging from typical drumlin to MSGL dimensions (**Fig. 7a**). Circular bedforms, i.e. bedforms with high I_{CIR}, tend to concentrate within the regional field of linear ribbed bedforms but are absent within the regional field of streamlined bedforms (**Figs. 7c, 10a**). The transition between ribbed and streamlined bedforms is gradual and characterized by an overall increase in sinuosity index (I_{SIN}) of bedform crest lines (**Fig. 7b**). Within this transitional field of bedforms, another transition from north to south is observed between predominantly flow-perpendicular ($I_{ELO} < 0$) and sinuous bedforms ($I_{SIN} > 0.1$), i.e. sinuous ribbed bedforms, and predominantly flow-parallel ($I_{ELO} > 0$) and sinuous bedforms ($I_{SIN} > 0.1$) (**Figs. 7a-b**).

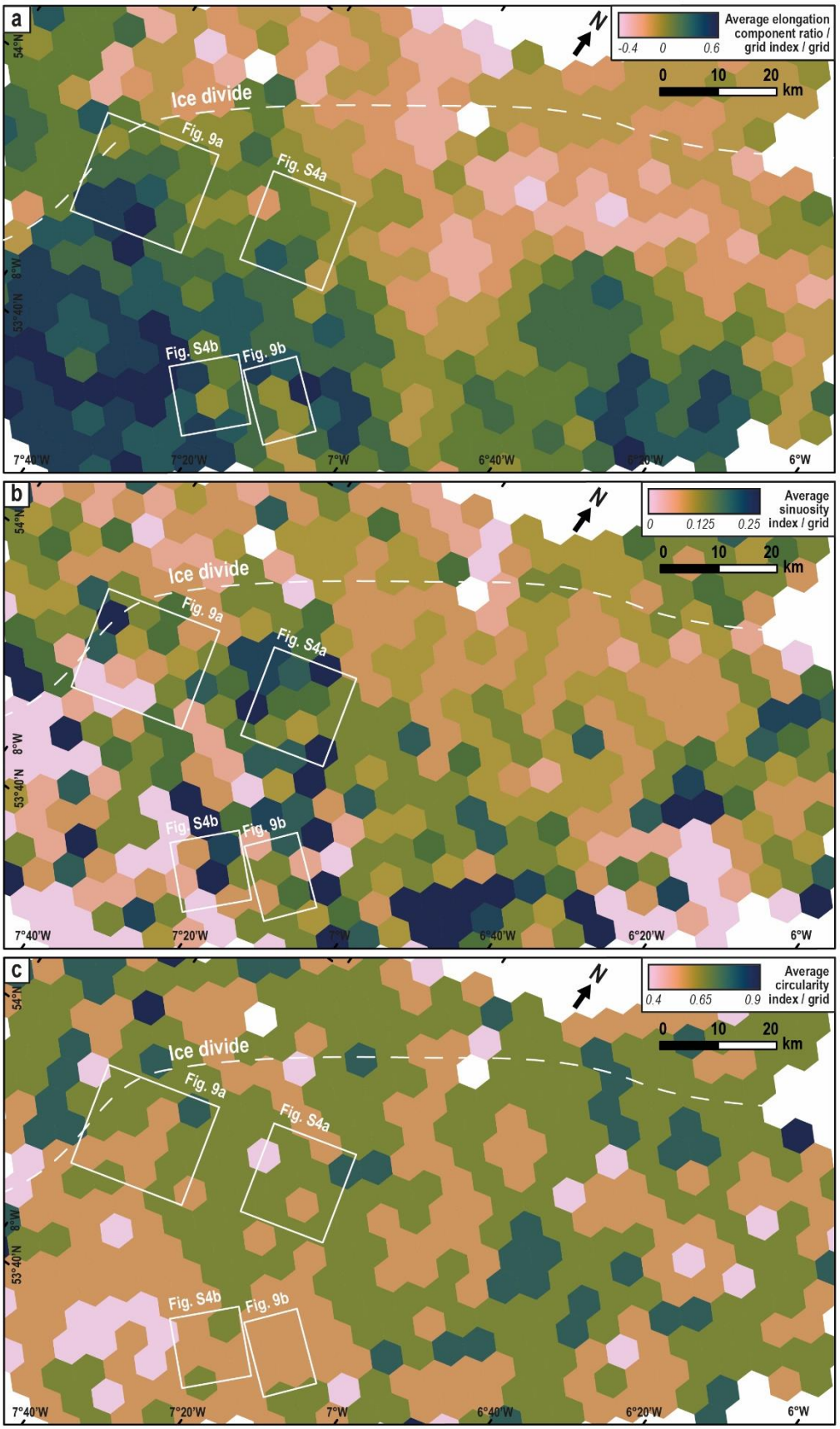

Figure 7. *Hexagonal grid maps of average morphometric indices (I_{ELO}, I_{SIN} and I_{CIR}) for bedforms observed along the IIS bed in northeastern Ireland. Sinuous bedforms (I_{SIN} > 0.1) without predominant elongation component (I_{ELO} ~ 0) gather in an intermediate position between linear ribbed bedforms (I_{SIN} < 0.1; I_{ELO} < 0) and streamlined bedforms (I_{SIN} < 0.1; I_{ELO} > 0). Circular bedforms, characterized by high circularity values, tend to gather in area where I_{ELO} is negative, in association with ribbed bedforms.*

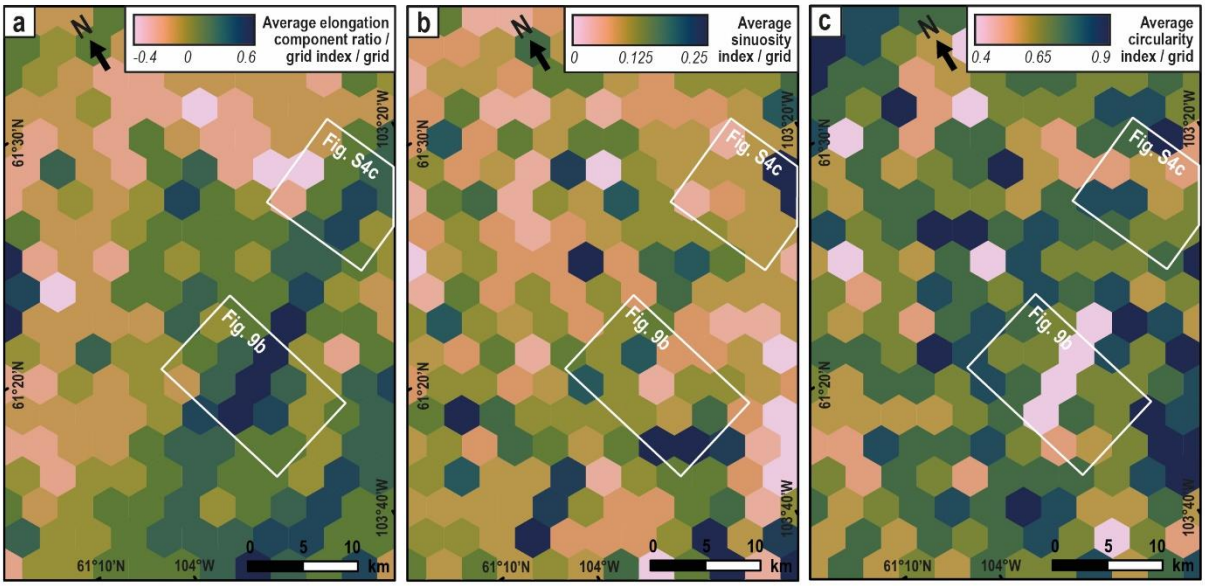

Figure 8. *Hexagonal grid maps of averaged morphometric indices (I_{ELO}, I_{SIN} and I_{CIR}) for bedforms observed along the LIS bed in Canada. Flow-parallel corridors of streamlined bedforms ($I_{ELO} > 0$, $I_{SIN} < 0.1$ and $I_{CIR} \sim 0.4$) alternate with corridors of ribbed bedforms ($I_{ELO} < 0$, $I_{SIN} < 0.1$ and $I_{CIR} > 0.65$) and sinuous bedforms ($I_{ELO} \sim 0$ and $I_{SIN} > 0.1$).*

Within a portion located in the western part of this transitional zone (**Fig. 9a**), an along-flow profile (A-A') and its associated graphs, displaying values of elongation component ratio (I_{ELO}) and sinuosity index (I_{SIN}) for each bedform, reveal a gradation from ribbed bedforms ($I_{ELO} < 0$) to streamlined bedforms ($I_{ELO} > 0$; $I_{SIN} \sim 0$), via sinuous ribbed bedforms ($I_{ELO} \leq 0$; $I_{SIN} > 0.1$) and sinuous predominantly flow-parallel bedforms ($I_{ELO} \geq 0$; $I_{SIN} > 0.1$). Within the same portion of this transitional zone (**Fig. 9a**), a symmetrical trend emerges from the lateral borders to the center of across-flow profiles (B-B'): the I_{ELO} increases from linear or sinuous ribbed bedforms to streamlined bedforms, through intermediate sinuous bedforms with I_{ELO} close to zero and high I_{SIN}.

Sinuous bedforms with an oblique orientation relative to the local ice flow direction frequently occur along such transitional zones, forming an "opening gate" pattern (**Fig. 10b**). Down-ice of these oblique and sinuous bedforms, streamlined bedforms are commonly aligned following the same oblique orientation forming an "en-echelon" pattern (**Fig. 10b**).

Within a portion located in the regional-scale field of streamlined bedforms in the southern part of the Irish study area (**Fig. 9b**), some linear and sinuous ribbed bedforms gather in sub-circular spots, approximately 3-km in diameter. Both along-flow and across-flow profiles of morphometric indices show striking symmetrical trends in bedform gradation: streamlined bedforms, predominantly flow-

parallel sinuous bedforms and linear / sinuous ribbed bedforms respectively occur from the borders to the core of the circular spot.

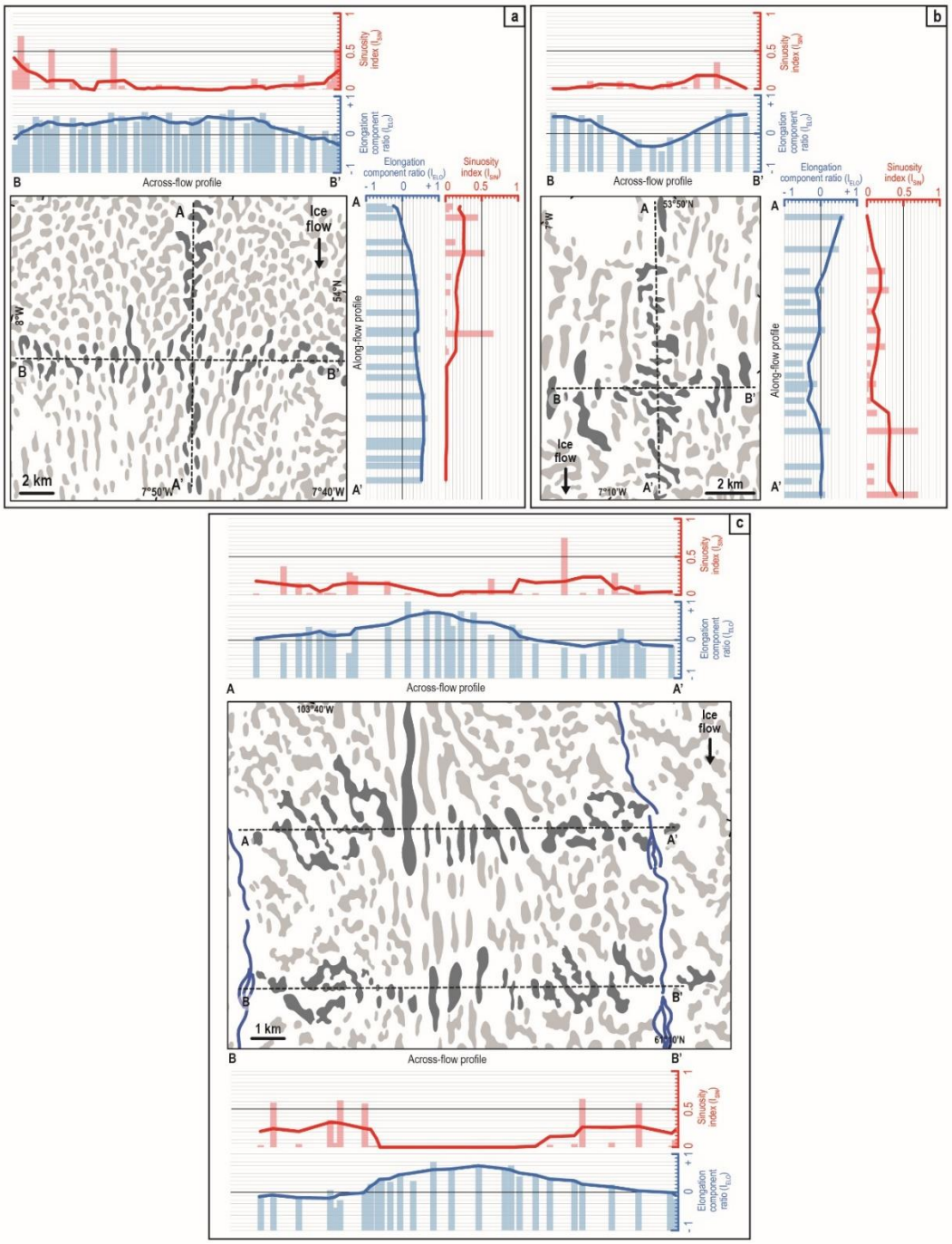

***Figure 9**. Interpretative maps with digitized bedforms of the Irish study area and associated profiles of elongation component ratio I_{ELO} and sinuosity index I_{SIN} along transitional sections between flow-perpendicular and flow parallel bedforms (cf. locations on **Figs. 7-8**). Profiles display raw values of morphometric variables for each bedforms (vertical bars) and moving average curves (5-values). (a) Sections located along the regional-scale transition between fields of linear ribbed bedforms (in the central / northern part of the study area) and streamlined bedforms (in the southwestern part of the study area). (b) Sections located within the regional-scale field of streamlined bedforms, in the southwestern part of the study area, and displaying local transition with spots of ribbed bedforms. (c) Across-flow sections intersect ribbed bedform tracts laterally alternating with streamlined bedform tracts. All profiles illustrate the progressive gradation, whether on regional- or local-scale, between linear flow-perpendicular bedforms ($I_{ELO} \leq 0$; $I_{SIN} \sim 0$) and linear flow-parallel bedforms ($I_{ELO} > 0$; $I_{SIN} \sim 0$) transitioning through sinuous bedforms with no dominant elongation component ($I_{ELO} \sim 0$; $I_{SIN} > 0$). Additional maps and morphometric profiles of similar transitional sections are provided in **Fig. S4**.*

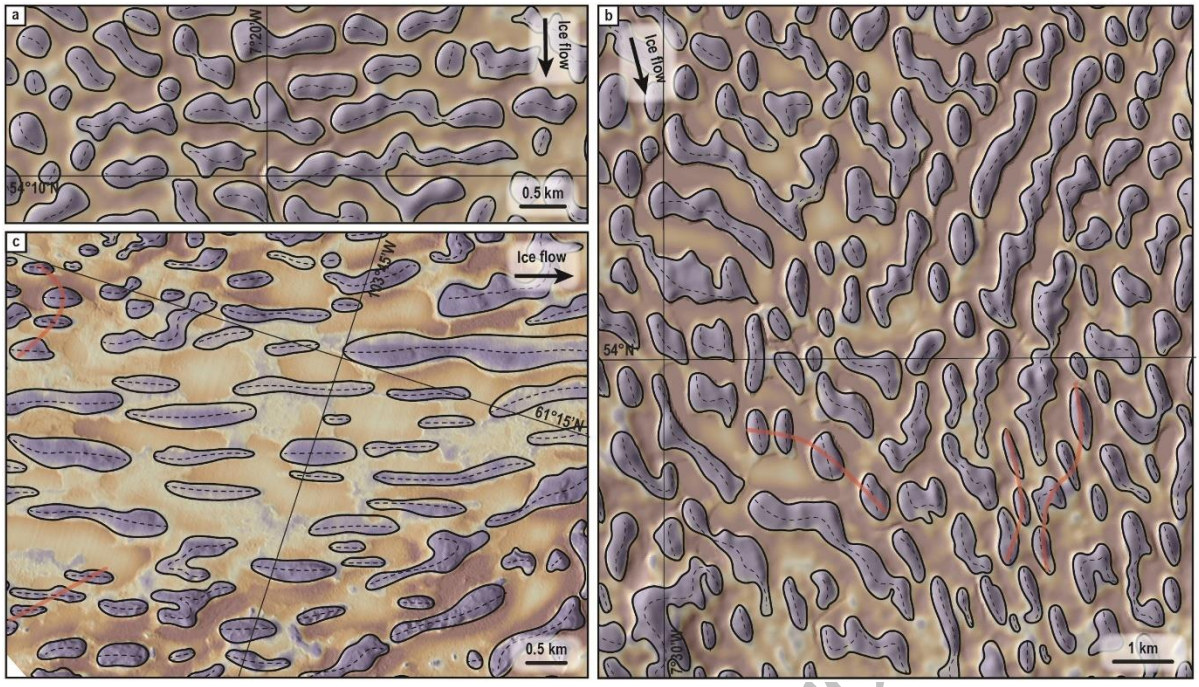

***Figure 10**. (a) Circular bedforms are scattered within a field of linear ribbed bedforms. (b) Sinuous bedforms with symmetric oblique orientations relative to the ice flow direction form an "opening gate" pattern. Down-ice of oblique bedforms, streamlined bedforms are aligned following the same oblique orientation forming an 'en-echelon' pattern (red lines). (c) Within a streamlined bedform tract elongated parallel to the ice flow direction, highly-elongated streamlined bedforms are laterally bounded by low-elongated streamlined bedforms, highlighting a progressive lateral diminution of I_{ELO}. Some of these low-elongated streamlined bedforms, associated down-ice with sinuous oblique bedforms with oblique orientation relative to the ice flow direction, exhibit an "en-echelon" pattern (red lines).*

3.2.2. Canada

This site is characterized by alternating tracts of streamlined and ribbed bedforms (**Figs. 5, 8**). These tracts are about 4-km wide and several tens of kilometers long; they are elongated parallel to the local ice flow direction and meltwater drainage features (eskers and meltwater channels). Along across-flow profiles to these tracts (**Fig. 9c**), tracts of ribbed bedforms characterized by low values of I_{ELO} and linear to low sinuous crest lines correlate with the position of drainage features. Streamlined bedforms characterized by a high I_{ELO} and linear crest lines are located in between drainage features. Laterally, sinuous ribbed bedforms and predominantly flow-parallel sinuous bedforms occur at the transition between linear ribbed bedform and streamlined bedform tracts. Some of these sinuous bedforms exhibit an obliquity to the local ice flow direction on both tract sides (**Fig. 10c**). Along across-flow profiles (**Fig. 9c**), streamlined bedforms with maximal I_{ELO} in the core of the corridor are bounded by streamlined bedforms with lower I_{ELO}, some of which exhibit an "en-echelon" pattern (**Fig. 10c**). The spatial gradation of I_{ELO} highlights there is no break in the distribution of streamlined bedforms morphometrics when increasing the I_{ELO}, which is materialized by an increasing LC_{MAX} with

a constant TC_{MAX} of 300 m (**Fig. 6a**). This gradation demonstrates the morphometric and spatial continuity between drumlins and MSGLs.

4. Discussion

The morphometric approach developed in this study, based on dimensionless indices allowing the possibility that bedforms can be sinuous and oblique to the ice flow directions, reveals that all the analyzed bedforms can be integrated in a morphometric continuum. Scatterplots (**Fig. 6**), maps (**Figs. 7-8**) and spatial transects of morphometric indices (**Fig. 9**) demonstrate a continuum of bedforms between: (i) circular bedforms, (ii) linear ribbed bedforms, (iii) streamlined bedforms and (iv) a variety of morphologically intermediate sinuous bedforms which were hitherto mostly interpreted as superimposed or multiphased bedforms.

4.1. A unifying sequence of bedform evolution

Based on the morphometric (**Fig. 6**) and spatial (**Figs. 7-10**) continuum of subglacial bedform shapes, we explore how the variations of the dimensionless morphometric indices could help deciphering the subglacial bedform evolution in a time and space grid. Keeping in mind the initial assumption that the formation of all bedforms is not necessarily synchronous but associated with constant ice flow trajectories, we suggest that circular to linear ribbed bedforms are the first bedforms to form, then become more sinuous and more elongated in the ice flow direction as they evolve. As the sinuosity index of their crest line (I_{SIN}) increases, we suggest that they then evolve into predominantly flow-parallel bedforms, until progressively paralleling the local ice flow direction to form streamlined bedforms with increasing elongation component ratio (I_{ELO}) (**Figs. 11-12**).

Three major assumptions are required to reconstruct the chronological frame of this bedform evolution: (1) ribbed bedforms, ranging from circular to linear forms, are incipient bedforms and their I_{ELO} is independent of their degree of bedform evolution; (2) sinuous bedforms are transitional bedforms between ribbed and streamlined bedforms along a sequence of increasing degree of bedform evolution; (3) streamlined bedforms arise from the fragmentation of transitional sinuous bedforms and their I_{ELO} increases as their degree of bedform evolution increases. We translate these assumptions into

an equation (***Eq. 1***) we applied on our bedform database (**Fig. 11**), representing our mathematical interpretation of the degree of bedform evolution:

$$Degree\ of\ bedform\ evolution = \left(\frac{\pi}{2} + \tan^{-1}\left(\frac{I_{ELO}}{I_{SIN}}\right)\right) \times (I_{ELO} + 1) \quad \textbf{(Eq. 1)}$$

Other propositions of equation quantifying the degree of bedform evolution and more details are presented in **Fig. S5**. These three assumptions and the bedform evolution sequence are discussed hereafter.

4.1.1. Ribbed bedforms with various elongation come first

4.1.1.1. Circular bedforms are circular forms of ribbed bedforms

Along the ordinate axis of the scatter plot in **Fig. 6,** circular bedforms are intermediate bedforms among the range of bedforms displaying linear crest lines (i.e. $I_{SIN} < 0.10$). This morphometric continuity is reflected (i) by their I_{ELO}, which is intermediate between those of linear ribbed bedforms and streamlined bedforms, and (ii) their average diameter, which is similar to the average TC_{MAX} of streamlined bedforms and to the average LC_{MAX} of linear ribbed bedforms. The morphometric continuity between linear ribbed, circular and streamlined bedforms corroborates the size and shape bedform continuum proposed by ***Ely et al. (2016)***. However, although circular bedforms are scattered within an area overlapping those of linear ribbed bedforms, circular bedforms are absent in the area where streamlined bedforms are abundant and do not particularly gather at the transition between ribbed and streamlined bedforms (**Fig. 7**). For our two study areas, those spatial distributions do not corroborate interpretations that circular bedforms are transitional forms between ribbed and streamlined bedforms (***Aario, 1977; Ely et al., 2016***). Considering the spatial relationships between subglacial bedforms, we suggest to insert circular bedforms in a morphometric and spatial continuum of ribbed bedforms ranging from circular to linear forms. In agreement with previous observations reported by ***Hättestrand (1997)***, ***Greenwood and Clark (2008)***, ***Möller and Dowling (2015)*** and ***Vérité et al. (2021, 2022),*** we therefore consider circular forms as circular ribbed bedforms.

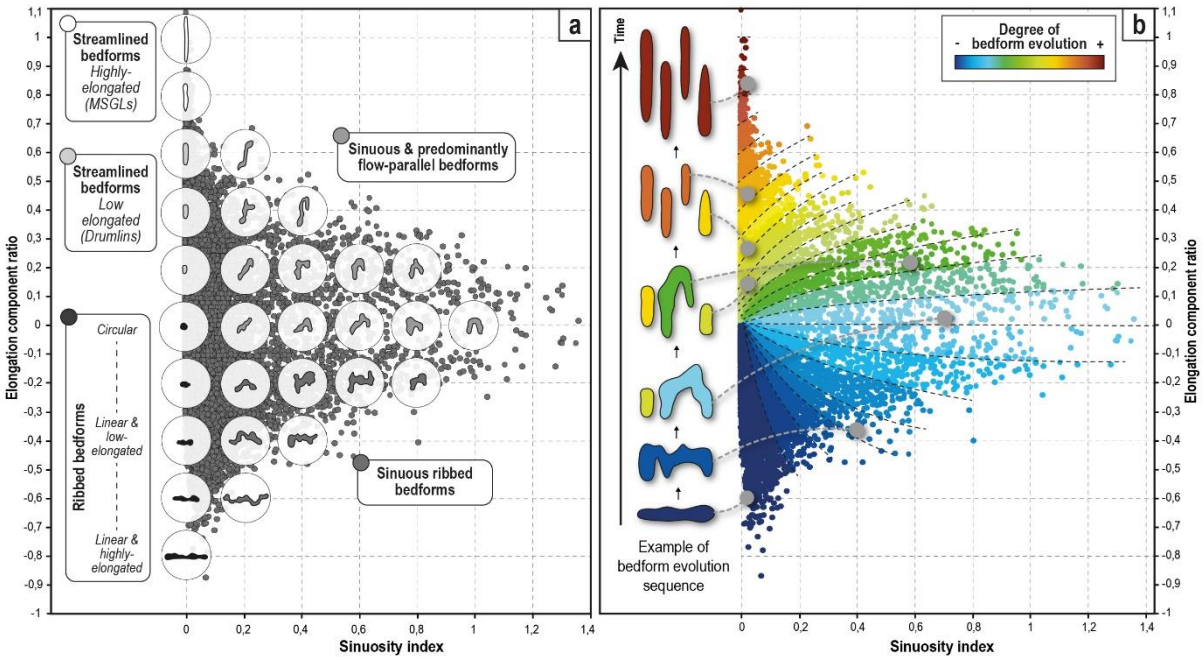

Figure 11. *(a) Plots of elongation component ratio (I_{ELO}) and sinuosity index (I_{SIN}) of bedforms mapped in this study with different bedform populations. (b) A degree of subglacial bedform evolution (from dark blue for the lower degree of evolution to red for the higher one) is calculated for each bedform using* ***Eq. 1*** *and is based on the evolution of elongation component ratio (I_{ELO}) and sinuosity index (I_{SIN}) along spatial sequences. Dotted black lines are graduations of the colored scale materializing the degree of bedform evolution. An example of morphological evolution sequence illustrates how a linear ribbed bedform progressively evolves and fragments through time into several sinuous and streamlined bedforms with increasing degrees of bedform evolution. The color of each bedform corresponds to the color associated with its degree of evolution; grey dots indicate the morphometric values of each bedform along the evolution sequence.*

4.1.1.2. Linear ribbed bedforms are incipient bedforms

Numerical models simulating the formation of subglacial bedforms demonstrate that ribbed bedforms with linear crest lines are the first bedforms to form, and constitute incipient bedforms in evolutionary sequences (***Chapwanya et al., 2011; Barchyn et al., 2016; Fannon et al., 2017***). Numerical models also demonstrated that circular bedforms can emerge from the random dislocation of ribbed bedforms without any increases of their width and sinuosity during the early stages of evolutionary sequences, constituting incipient bedforms just as ribbed bedforms (***Fannon, 2020 p.139–140; Ely et al., 2022***). Similarly, physical simulations demonstrated the synchronous formation of ribbed bedforms with various values of their maximal transverse components and various shapes, ranging from circular to highly-elongated forms (***Vérité et al., 2021, 2022***). Considering (i) these modeling observations and (ii) the high overlap between the spatial distribution of circular and linear ribbed bedforms with variable elongation (**Fig. 7**), we propose that incipient ribbed bedforms arise with a random maximal transverse component. Corroborating works from ***Hättestrand (1997)*** and ***Möller and Dowling (2015)*** interpreting a continuum of ribbed bedforms from circular to transverse

and elongated forms as resulting from a single process, we propose that ribbed bedforms with linear crest lines correspond to the first stage of subglacial bedform evolution (**Fig. 12a**), whatever their size and shape (***Dunlop and Clark, 2006; Greenwood and Kleman, 2010, Ely et al., 2016***).

4.1.2. Ribbed bedforms evolve into sinuous transitional bedforms

According to the initial size and shape of the ribbed bedform and to the later stages of bedform transformation, an infinite number of bedform evolutions can be followed (**Fig. 11**), leading to variations in the metrics of bedform sequences (**Fig. 12 ;** three of them are represented). Sequences n° 2 and 3 aim to respectively represent the evolution of a low-elongated and a highly-elongated ribbed bedform, and are built using typical bedform assemblages observed along spatial sequences. Based on evolution sequences n°2 and 3, we suggest that elongated ribbed bedforms, characterized by a linear crest line when they initially form, become increasingly sinuous (with increasing I_{ELO}) as their degree of evolution increases and as they are initially highly-elongated (**Fig. 12**). Numerical simulations of subglacial bedforms demonstrated that, whatever the glaciological and hydrological conditions simulated, ribbed bedforms become increasingly stretched towards the ice flow direction, sinuous and oblique as they evolve before dislocating into streamlined bedforms (Supplementary materials of ***Fannon et al. 2017; Fannon, 2020 p.139; Ely et al., 2022***). Those numerical simulations, supporting our model of bedform evolution, agree with recent physical modeling works describing increasingly sinuous and oblique ribbed bedform through experimental runs (***Vérité et al., 2021, 2022***). These works support the hypothesis – postulated from scatterplots (**Fig. 6**) and morphometrical transects through bedform fields (**Fig. 9**) – that sinuous ribbed bedforms and predominantly flow-parallel sinuous bedforms could represent transitional bedforms resulting from the evolution of linear ribbed bedforms (**Figs. 12b-c**). This interpretation also correlates with the description of complex bedforms in intermediate positions along spatial sequences unifying ribbed and streamlined bedforms along palaeo-ice sheet beds (***Carl, 1978; Markgren & Lassila, 1980; Aylsworth & Shilts, 1989; Knight et al., 1999***).

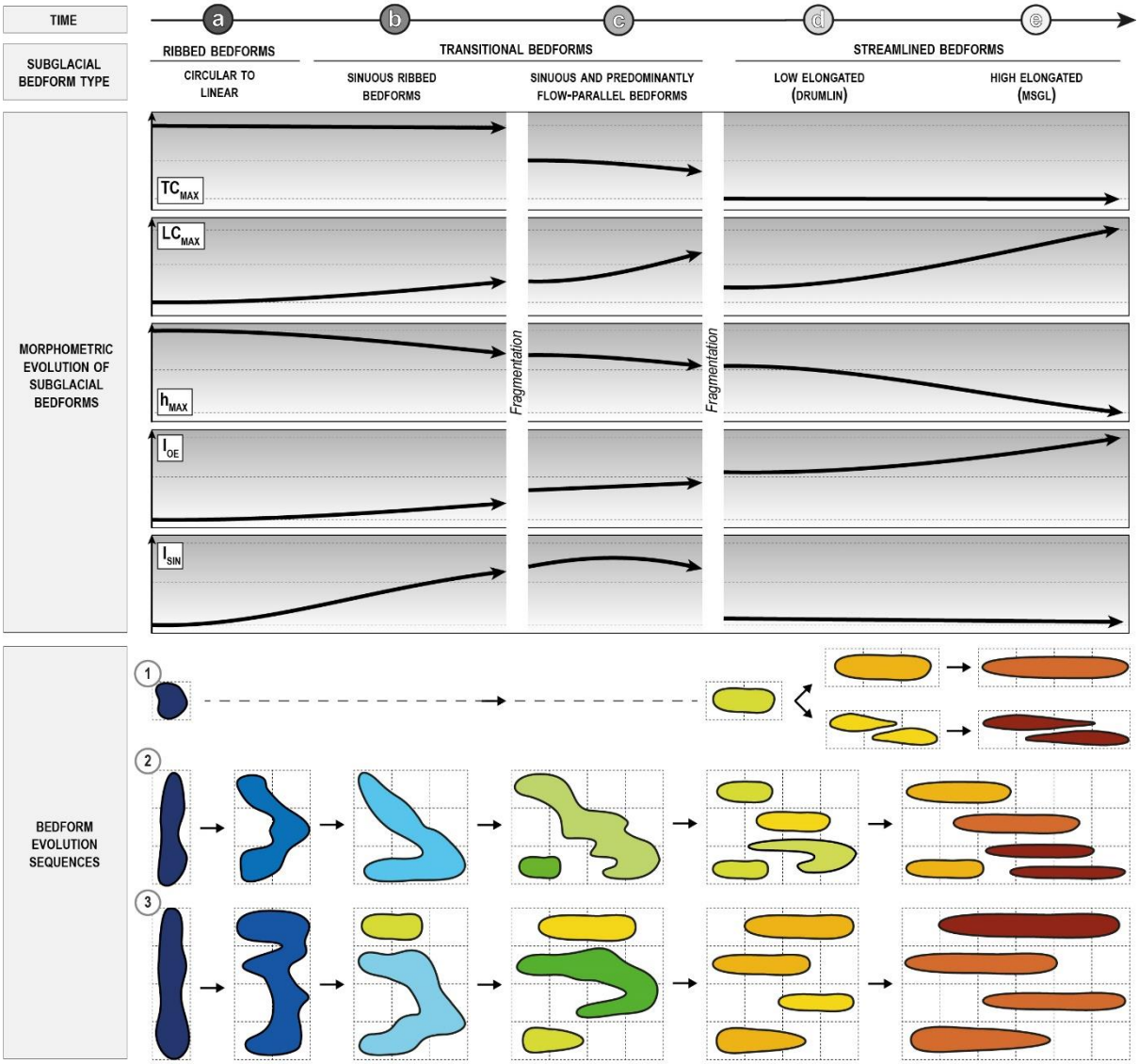

***Figure 12**. Model of morphological evolution of subglacial bedforms, derived from the morphometric and spatial continuum observed in our study. Subglacial bedforms initiate as circular to linear ribbed bedforms. Linear ribbed bedforms progressively evolve through complex transitional bedforms with variable sinuosities and orientations, towards increasingly elongated streamlined bedforms; while circular ribbed bedforms progressively evolve into a unique or several streamlined bedforms without complex transitional bedforms. The degree of bedform evolution, defined from the combination of their I_{ELO} and I_{SIN}, is a quantitative measure of this progressive evolution. Three examples of bedform evolution sequences are proposed depending on the initial I_{ELO} of the ribbed bedform (evolution sequence n°3 is presented in **Fig. 11b**). The color of each bedform corresponds to the color associated with its degree of evolution indicated in **Fig. 11b**.*

4.1.3. Streamlined bedforms arise from sinuous transitional bedform fragmentation and are increasingly elongated as they evolve

In Ireland and Canada, sinuous oblique bedforms and "en-echelon pattern" of drumlins – examples of which have been independently mentioned in the literature (***Shaw, 1983; Stokes et al., 2016; Clark et al., 2018***) – are observed along transition zones between ribbed and streamlined bedforms (**Figs. 10b-c**). Similar examples of sinuous oblique bedforms fragmenting into streamlined bedforms with en-echelon patterns have been numerically simulated by ***Fannon et al. (2017)***, ***Fannon***

(2020; p.139) and ***Ely et al. (2022)***, suggesting that streamlined bedforms derive from the fragmentation of sinuous, sometimes oblique bedforms (**Fig. 12**; evolution sequence n°2 and 3). Our results strongly support these observations and simulations. On average, the maximal transverse components (TC_{MAX}) of transitional bedforms and streamlined bedforms are respectively half and a quarter the TC_{MAX} measured for ribbed bedforms. The evolution of the maximal longitudinal component (LC_{MAX}) is anti-correlated with both TC_{MAX} and amplitudes (h_{MAX}) illustrating the progressive elongation parallel to the ice flow direction and thinning of bedforms. The process of bedform evolution leading to inversion of the dominant component (i.e. TC_{MAX} towards LC_{MAX}) is concomitant with an initial increase in bedform sinuosity. The fragmentation of sinuous bedforms in response to sustained stretching subdivides the bedforms into multiple smaller and less sinuous entities (**Figs. 12c-d**).

The fragmentation first leads to the formation of distinct and individualized low-elongated and flow-parallel bedforms we consider as being proto-drumlins (***Clark et al., 2009***). **Figure 6** shows there is no break in the distribution of streamlined bedforms morphometrics when increasing the $I_{ELO,}$ demonstrating continuity between drumlins and MSGLs. In Ireland and Canada, this continuity is also spatial as increasing I_{ELO} gradients – which is materialized by an increasing LC_{MAX} with a constant TC_{MAX} (~300 m) – occur parallel (i.e. in the down-ice direction; **Fig. 9a**) or transverse to the local ice flow direction (**Fig. 9c**). In addition to several studies highlighting the spatial (***Aario, 1977; Boyce and Eyles, 1991; Hart, 1999; Stokes and Clark, 2002; Briner, 2007; Sookhan et al., 2021***) and morphometric (***Rose, 1987***; ***Clark et al., 2009***; ***Stokes et al., 2013; Ely et al., 2016)*** continuity between drumlins and MSGLs, we quantitatively demonstrate that the intensity of streamlined bedform elongation parallel to the ice flow direction illustrates their degree of evolution (**Figs. 11-12**).

4.1.4. Other potential evolutionary sequences

Complex sinuous bedforms, corresponding to transitional bedforms, do not systematically occur within subglacial bedform assemblages along palaeo-ice sheet beds, suggesting that other evolutionary sequences without sinuous bedforms should also exist.

Considering evolutionary sequence n°1 (**Fig. 12**), initial ribbed bedforms with a circular shape will evolve into single or multiple increasingly elongated streamlined bedforms, without sinuous

transitional bedforms. This evolutionary sequence agrees with the continuum of streamlined bedforms proposed by ***Sookhan et al. (2021)***, which demonstrate that sub-circular and large drumlins may subdivide into smaller and more elongated ones without transitional sinuous forms. They indeed demonstrate that the evolution / subdivision of a large drumlin results in contiguous drumlins with individual linear crest lines. ***Ely et al. (2018)*** also suggested that drumlins emerge as circular forms before growing, migrating, elongating and potentially coarsening through drumlin amalgamation. Except for coarsening processes that are not included in this study, this is consistent with the evolution sequence n°1 proposed in **Figure 12**. The existence of such evolutionary sequences, not requiring the initial presence of ribbed bedforms, suggests that streamlined bedforms can form self-organized periodic patterns (i.e. regular spacing and alignment) despite the absence of preliminary sinuous bedform fragmentation processes, as suggested by ***Spagnolo et al. (2017)*** and ***Ely et al. (2018)***.

4.2. Sinuous bedforms vs superimposed bedforms along palaeo-ice sheet beds: a time-transgressive issue

This model of bedform continuum and the interpretation of sinuous/complex bedforms as transitional bedforms between ribbed and streamlined bedforms rely on the main and strong assumption of a steady ice flow configuration. The formation of most complex bedforms could alternatively be explained by multiple and asynchronous ice flow trajectories.

In Ireland and Canada (**Figs. 4-5**), the "steady" assumption is supported by the lack of cross-cutting flow-sets of streamlined bedforms within areas of several thousands of square kilometers around the study sites. Complex bedforms have alternatively been interpreted as superimposed drumlins on a pre-existing parent ice-remolded bedform (e.g. ***Clark, 1993***), thus suggesting cross-cutting ice flow directions. We rather suggest that complex bedforms display shapes and orientations consistent with their transitional position along spatial evolutionary sequences deciphered from morphometrical analysis, especially when surrounding bedform fields do not record converging streamlined bedforms. The observation of "opening gate" patterns (see **Fig. 9**) associated with some oblique bedforms displaying a symmetric pattern with respect to the ice flow direction could be consistent with at least three cross-cutting ice flow direction suggested by "superimposed drumlins".

However, multiple ice flow trajectories along both selected sites are more likely not reliable for two main reasons. First, such hypothetical changes in ice flow directions are not consistent with the most recent reconstruction of ice flow geometry over the Irish Ice Sheet when ice was covering the study area, even during migration of ice divides and reorganization of the ice flow geometry during the early stages of deglaciation (***Clark et al. 2022***). Second, the preservation potential of multiple generations of bedforms composed of unconsolidated sediments is questionable considering that changes in flow trajectories are generally associated with changes in ice flow dynamics and reconfiguration of the subglacial hydrological system, which could favor erosion, reshaping and even erasing of preexisting bedforms generations rather than their preservation (e.g. ***Clark, 1999; Benediktsson et al., 2022***).

The steady flow trajectory and the bedform continuum model we determine using our database is not ubiquitous and it should be noted that complex subglacial forms might also derive from the remolding of pre-existing bedforms and/or the superimposition of bedform generations driven by changes in ice flow direction (e.g. ***Rose & Letzer, 1977; Rose, 1987; Clark, 1993; Knight, 1997; Stokes et al., 2006a***). Within study areas where morphological evidence would clearly indicate time-transgressive subglacial records with changes in ice flow directions, the evolutionary models we determined from our database would indeed not be relevant to reconstruct past glacial dynamics. However, the areas presented in this article demonstrate that the integration of these complex bedforms into a single continuum model could help in revising the number of ice-sheet flow trajectories currently envisaged in Ireland (***Greenwood and Clark, 2009a; Clark et al., 2022***), in Canada (***Winsborrow et al., 2004; De Angelis & Kleman, 2007***) and probably in many other areas.

4.3. Glaciodynamics significance of the bedform evolution degree

The sequences of bedform evolution have sometimes been interpreted as spatial variations in the duration of ice streaming process (***Boyce and Eyles, 1991; Jamieson et al., 2016; Zoet et al., 2021***), bed lithology (***Aylsworth and Shilts, 1989; Wellner et al., 2001; O Cofaigh et al., 2002; Greenwood and Clark, 2010; McKenzie et al., 2022***), bed topography (***Bouchard, 1989; Franke et al., 2020***), bed thickness (***Kerr & Eyles, 2007; Barchyn et al., 2016***) or meltwater pressure (***Shaw, 2002***; ***Lewington, 2020***). In most cases, they have been interpreted as spatial variations in ice flow velocity from the

onset area to the ice stream core (***Dyke et al., 1992; King et al., 2007***) and even along or across the ice stream itself (***Aario, 1977; Hart, 1999; Briner, 2007; Stokes et al., 2013; Hillier et al., 2016; Jamieson et al., 2016; Hermanowski et al., 2019; Van Landeghem & Chiverrell, 2020; Sookhan et al., 2021, 2022***).

In Ireland, streamlined bedform tracts – several 10s of kilometers long and wide – have been interpreted as palaeo-corridors of fast ice flow (***Synge and Stephens, 1960; Stokes and Clark, 1999; Greenwood and Clark, 2009a***), which probably correspond to palaeo-ice streams draining the Lowland Ice Dome between 20 and 17 ka BP (***Clark et al., 2022***). Morphometric and spatial analyses conducted in Ireland suggest that the bedform distribution reveals longitudinal and lateral gradients of bedform evolution relative to the ice flow direction (**Figs. 7-8**), certainly recording ice flow velocity pattern along and across an ice stream. Indeed, the transition between slow ice near the ice dome (i.e. onset area) and at ice stream margins (i.e. shear margins) to fast ice in the ice stream core is respectively recorded through transitions between ribbed, sinuous and streamlined bedforms (**Fig. 9b**). Our model, encompassing the degree of bedform evolution in a spatio-temporal continuum, is convincing as it can be explained by transitions in ice flow velocity classically monitored in modern ice streams (e.g. ***Sergienko & Hindmarsh, 2013; Zheng et al., 2019***).

Small fields of linear to sinuous ribbed bedforms contained within streamlined bedform tracts in Ireland (**Fig. 10**) indicate abrupt and very localized changes in the degree of bedform evolution. We interpret this local anomaly in bedform evolution as the morphological expression of slow ice patches within fast-flowing ice corridors, as has commonly been reported for ice stream sticky spots (***Alley, 1993).*** We notice that palaeo-sticky spots have mainly been recognized through the superposition of ribbed bedforms on top of streamlined bedforms (***Stokes et al., 2006b, 2007, 2016***). There are no cross-cutting relationships or superposition in the sticky spots revealed in Ireland, instead we suggest that streamlined bedforms and ribbed bedforms are synchronous and that patches of bedform of lower evolution reveal sustained sticky conditions related to nearby bedrock topographic highs.

In Canada, previous studies suggest that the position of the study area below the Keewatin Ice Dome intersects meltwater corridors that developed below the retreating Laurentide Ice Sheet (***Storrar et al., 2013; Lewington et al., 2020***). Moreover, ***Lewington (2020)*** suggested that corridors of ribbed

bedforms below the Keewatin – which were identified alternating with corridors of drumlins by ***Shilts et al., 1987*** and ***Aylsworth & Shilts (1989)*** – correspond to potential geomorphic markers of meltwater corridors. This suggests that the lateral variations in bedform morphologies observed across well-defined meltwater drainage features indicate the influence of meltwater pressure variations on the degree of bedform evolution (**Fig. 11**).

Assuming constant ice-flow trajectories and the model of bedform continuum is correct, the spatial diversity of bedform shapes, dimensions and orientation observed in Ireland and Canada indicates various degree of bedform evolution relative to spatial variations in subglacial conditions (e.g. ice flow velocity, bedrock characteristics, meltwater pressure).

5. Conclusion

Combined mapping and morphometric analysis of 13,500 subglacial bedforms enabled the morphological evolution of subglacial bedforms to be explored.

First, a new morphometric approach – based on the computation of the circularity index (I_{CIR}), sinuosity index (I_{SIN}) and elongation component ratio (I_{ELO}) of subglacial bedforms – reveals a morphometric and spatial continuum between ribbed bedforms (i.e. circular to elongated, flow-transverse and linear forms), streamlined bedforms (i.e. drumlins and MSGLs) and sinuous bedforms with various shapes and orientations (i.e. sinuous ribbed bedforms and predominantly flow-parallel sinuous bedforms). Complex, oblique and sinuous bedforms, which have been excluded from most existing models of subglacial continuum and commonly interpreted as resulting from the remolding/superimposition of more simple and younger bedforms, are part of this continuum and can form under the same ice flow trajectory as ribbed and streamlined bedforms.

Second, we interpreted this morphological and spatial continuum as the expression of evolutionary sequences between a diversity of ribbed bedforms, ranging from circular to linear transverse, and streamlined bedforms. Intermediate sinuous bedforms, recording the progressive realignment and elongation in the ice flow direction, can correspond to transitional bedforms that result from the stretching of linear ribbed bedforms and fragment into several streamlined bedforms. Evolutionary sequences between circular ribbed bedforms and streamlined bedforms are also thought

to exist without an intermediate stage of sinuous bedforms. The degree of bedform evolution along these evolutionary sequences can be quantified by a morphometric variable based on the elongation component ratio and the sinuosity index.

The results of this study are consistent with previous works on the subglacial bedform continuum (***Lundqvist, 1970; Aario, 1977; Rose, 1987; Ely et al., 2016, 2022***, ***Sookhan et al., 2021***), but go further into the integration of the whole morphological diversity of subglacial bedforms and in the description of transitional steps characterizing the bedform re-alignment between flow-transverse ribbed bedforms and flow-parallel streamlined bedforms. The spatial relationships between bedform evolutionary sequences reported in Ireland and Canada and their assumed glaciological contexts (e.g. ice flow velocity, meltwater pressure, bed topography and lithology) suggest the degree of bedform evolution could be used to (1) explore factors controlling subglacial bedform formation and evolution and (2) reconstruct the past glacial dynamics with greater detail. This work opens up new perspectives to bridge the gap between subglacial bedform morphology, subglacial processes and ice dynamics. Further work is needed to explore the genetic significance of this morphometric continuum that could contribute to increase the resolution of reconstructions of past glacial dynamics and ice-meltwater-bed interactions.

Acknowledgment

This study is part of the Ice-Collapse project (The dynamics of ice sheet collapse in deglaciation periods) funded by the French Agence Nationale de la Recherche through grant ANR-18-CE01-0009.

Data availability

All datasets used in this paper are available from the corresponding author on request.

Declaration of competing interests

The authors declare that they have no conflict of interest.

References

Aario, R. (1977). Classification and terminology of morainic landforms in Finland. Boreas, 6(2), 87-100.

Alley, R. B., 1993. In search of ice-stream sticky spots. Journal of Glaciology 39 (133), 447–454.

Aylsworth, J. M., & Shilts, W. W. (1989). Bedforms of the Keewatin ice sheet, Canada. Sedimentary Geology, 62(2-4), 407-428.

Barchyn, T. E., Dowling, T. P., Stokes, C. R., & Hugenholtz, C. H. (2016). Subglacial bed form morphology controlled by ice speed and sediment thickness. Geophysical Research Letters, 43(14), 7572-7580.

Batchelor, C. L., Margold, M., Krapp, M., Murton, D. K., Dalton, A. S., Gibbard, P. L., Stokes, C. R., Murton, J. B., Manica, A., 2019. The configuration of Northern Hemisphere ice sheets through the Quaternary. Nature communications 10 (1), 3713.

Benediktsson, Í. Ö., Aradóttir, N., Ingólfsson, Ó., & Brynjólfsson, S. (2022). Cross-cutting palaeo-ice streams in NE-Iceland reveal shifting Iceland Ice Sheet dynamics. Geomorphology, 396, 108009.

Birch, C. P., Oom, S. P., & Beecham, J. A. (2007). Rectangular and hexagonal grids used for observation, experiment and simulation in ecology. Ecological modelling, 206(3-4), 347-359.

Bouchard, M. A., 1989. Subglacial landforms and deposits in central and northern Quebec, Canada, with emphasis on Rogen moraines. Sedimentary Geology 62 (2–4), 293–308.

Boulton, G. S. 1987. A theory of drumlin formation by subglacial sediment deformation. In: Menzies, J. & Rose, J. (eds) Drumlin Symposium. Balkema, Rotterdam, 25-80.

Boyce, J. I., & Eyles, N. (1991). Drumlins carved by deforming till streams below the Laurentide ice sheet. Geology, 19(8), 787-790.

Briner, J. P. (2007). Supporting evidence from the New York drumlin field that elongate subglacial bedforms indicate fast ice flow. Boreas, 36(2), 143-147.

Brown, V. H., Stokes, C. R., & O'Cofaigh, C. (2011). The glacial geomorphology of the north-west sector of the Laurentide Ice Sheet. Journal of Maps, 7(1), 409-428.

Burgess, D. O., Shaw, J., & Eyton, J. R. (2003). Morphometric comparisons between Rogen terrain and hummocky terrain. Physical Geography, 24(4), 319-336.

Canals, M., Urgeles, R., & Calafat, A. M. (2000). Deep sea-floor evidence of past ice streams off the Antarctic Peninsula. Geology, 28(1), 31-34.

Carl, J. D. (1978). Ribbed moraine–drumlin transition belt, St. Lawrence Valley, New York. Geology, 6(9), 562-566.

Chapwanya, M., Clark, C. D., & Fowler, A. C. (2011). Numerical computations of a theoretical model of ribbed moraine formation. Earth Surface Processes and Landforms, 36(8), 1105-1112.

Clark, C. D. (1993). Mega-scale glacial lineations and cross-cutting ice-flow landforms. Earth surface processes and landforms, 18(1), 1-29.

Clark, C. (1999). Glaciodynamic context of subglacial bedform generation and preservation. Annals of Glaciology, 28, 23-32. doi:10.3189/172756499781821832

Clark, C. D., Hughes, A. L., Greenwood, S. L., Spagnolo, M., & Ng, F. S. (2009). Size and shape characteristics of drumlins, derived from a large sample, and associated scaling laws. Quaternary Science Reviews, 28(7-8), 677-692.

Clark, C. D., Ely, J. C., Spagnolo, M., Hahn, U., Hughes, A. L., & Stokes, C. R. (2018). Spatial organization of drumlins. Earth Surface Processes and Landforms, 43(2), 499-513.

Clark, C. D., Ely, J. C., Hindmarsh, R. C. A., Bradley, S., Igneczi, A., Fabel, D., ´ O Cofaigh, C., Chiverrell, R. C., Scourse, J., Benetti, S., Bradwell, T., Evans, D. J. A., Roberts, D. H., Burke, M., Callard, S. L., Medialdea, A., Saher, M., Small,D., Smedley, R.K., Gasson, E., Gregoire, L., Gandy,N.,Hughes, A. L. C., Ballantyne, C., Bateman,M.D., Bigg, G. R., Doole, J., Dove, D., Duller, G. A. T., Jenkins, G. T. H., Livingstone, S. L., McCarron, S., Moreton, S., Pollard, D., Praeg, D., Sejrup, H. P., van Landeghem, K. J. J. & Wilson, P. (2022). Growth and retreat of the last British–Irish Ice Sheet, 31 000 to 15 000 years ago: the BRITICE-CHRONO reconstruction.Boreas, Vol. 51, pp. 699–758. https://doi.org/10.1111/bor.12594. ISSN 0300-9483.

Cowan, W. R. (1968). Ribbed moraine: till-fabric analysis and origin. Canadian Journal of Earth Sciences, 5(5), 1145-1159.

De Angelis, H., & Kleman, J. (2007). Palaeo-ice streams in the Foxe/Baffin sector of the Laurentide Ice Sheet. Quaternary Science Reviews, 26(9-10), 1313-1331.

Doornkamp, J. C., & King, C. A. (1971). Numerical analysis in geomorphology: an introduction. Hodder Education.

Dowling, T. P., Spagnolo, M., & Möller, P. (2015). Morphometry and core type of streamlined bedforms in southern Sweden from high resolution LiDAR. Geomorphology, 236, 54-63.

Dunlop, P., & Clark, C. D. (2006). The morphological characteristics of ribbed moraine. Quaternary Science Reviews, 25(13-14), 1668-1691.

Dyke, A. S., Vincent, J. S., Andrews, J. T., Dredge, L. A., & Cowan, W. R. (1989). The Laurentide Ice Sheet and an introduction to the Quaternary geology of the Canadian Shield. Quaternary Geology of Canada and Greenland, R.J. Fulton

Dyke, A. S., Morris, T. F., Green, D. E., & England, J. (1992). Quaternary geology of Prince of Wales island, arctic Canada.

Ely, J. C., Clark, C. D., Spagnolo, M., Stokes, C. R., Greenwood, S. L., Hughes, A. L., Dunlop, P., & Hess, D. (2016). Do subglacial bedforms comprise a size and shape continuum?. Geomorphology, 257, 108-119.

Ely, J. C., Clark, C. D., Spagnolo, M., Hughes, A. L., & Stokes, C. R. (2018). Using the size and position of drumlins to understand how they grow, interact and evolve. Earth Surface Processes and Landforms, 43(5), 1073-1087.

Ely, J. C., Stevens, D., Clark, C. D., & Butcher, F. E. G (2022). Numerical modelling of subglacial ribs, drumlins, herringbones, and mega-scale glacial lineations reveals their developmental trajectories and transitions. Earth Surface Processes and Landforms.

Eyles, N. (2012). Rock drumlins and megaflutes of the Niagara Escarpment, Ontario, Canada: a hard bed landform assemblage cut by the Saginaw–Huron Ice Stream. Quaternary Science Reviews, 55, 34-49.

Eyles, N., Putkinen, N., Sookhan, S., & Arbelaez-Moreno, L. (2016). Erosional origin of drumlins and megaridges. Sedimentary Geology, 338, 2-23.

Fannon, J. S., Fowler, A. C., & Moyles, I. R. (2017). Numerical simulations of drumlin formation. Proceedings of the Royal Society A: Mathematical, Physical and Engineering Sciences, 473(2204), 20170220.

Fannon, J. S., 2020. Mathematical Modelling of Subglacial Bedform Formation and Dense Granular Flows. University of Limmerick. Limerick Ph.D.

Folk, R. L. (1968). Petrology of sedimentary rocks: Hemphill's. Austin, Texas, vol. 170, p. 85.

Franke, S., Jansen, D., Binder, T., Dörr, N., Helm, V., Paden, J., ... & Eisen, O. (2020). Bed topography and subglacial landforms in the onset region of the Northeast Greenland Ice Stream. Annals of Glaciology, 61(81), 143-153.

Greenwood, S. L., & Clark, C. D. (2008). Subglacial bedforms of the Irish ice sheet. Journal of Maps, 4(1), 332-357.

Greenwood, S. L., & Clark, C. D. (2009a). Reconstructing the last Irish Ice Sheet 1: changing flow geometries and ice flow dynamics deciphered from the glacial landform record. Quaternary Science Reviews, 28(27-28), 3085-3100.

Greenwood, S. L., & Clark, C. D. (2009b). Reconstructing the last Irish Ice Sheet 2: a geomorphologically-driven model of ice sheet growth, retreat and dynamics. Quaternary Science Reviews, 28(27-28), 3101-3123.

Greenwood, S. L., Clark, C. D., 2010. The sensitivity of subglacial bedform size and distribution to substrate lithological control. Sedimentary Geology 232 (3–4), 130–144.

Greenwood, S. L., & Kleman, J. (2010). Glacial landforms of extreme size in the Keewatin sector of the Laurentide Ice Sheet. Quaternary Science Reviews, 29(15-16), 1894-1910.

Hart, J. K. (1999). Identifying fast ice flow from landform assemblages in the geological record: a discussion. Annals of Glaciology, 28, 59-66.

Hättestrand, C. (1997). Ribbed moraines in Sweden—distribution pattern and palaeoglaciological implications. Sedimentary Geology, 111(1-4), 41-56.

Hermanowski, P., Piotrowski, J. A., & Szuman, I. (2019). An erosional origin for drumlins of NW Poland. Earth Surface Processes and Landforms, 44(10), 2030-2050.

Hill, A. R. (1973). The distribution of drumlins in County Down, Ireland. Annals of the Association of American Geographers, 63(2), 226-240.

Hillier, J. K., & Smith, M. (2008). Residual relief separation: digital elevation model enhancement for geomorphological mapping. Earth Surface Processes and Landforms, 33(14), 2266-2276.

Hillier, J. K., Kougioumtzoglou, I. A., Stokes, C. R., Smith, M. J., Clark, C. D., Spagnolo, M. S., 2016. Exploring explanations of subglacial bedform sizes using statistical models. Plos one 11 (7), e0159489.

Hollingworth, S. E. (1931). The glaciation of western Edenside and adjoining areas and the drumlins of Edenside and the Solway basin. Quarterly Journal of the Geological Society, 87(1-4), 281-359.

Jamieson, S. S., Stokes, C. R., Livingstone, S. J., Vieli, A., Cofaigh, C. Ó., Hillenbrand, C. D., & Spagnolo, M. (2016). Subglacial processes on an Antarctic ice stream bed. 2: Can modelled ice dynamics explain the morphology of mega-scale glacial lineations?. Journal of Glaciology, 62(232), 285-298.

Johnson, M. D., Schomacker, A., Benediktsson, Í. Ö., Geiger, A. J., Ferguson, A., Ingólfsson, Ó., 2010. Active drumlin field revealed at the margin of Múlajökull, Iceland: a surge-type glacier. Geology 38 (10), 943–946.

Kerr, M., & Eyles, N. (2007). Origin of drumlins on the floor of Lake Ontario and in upper New York State. Sedimentary Geology, 193(1-4), 7-20.

King, E. C., Woodward, J., & Smith, A. M. (2007). Seismic and radar observations of subglacial bed forms beneath the onset zone of Rutford Ice Stream, Antarctica. Journal of Glaciology, 53(183), 665-672.

Knight, J. (1997). Morphological and morphometric analyses of drumlin bedforms in the Omagh Basin, north central Ireland. Geografiska Annaler: Series A, Physical Geography, 79(4), 255-266.

Knight, J., Stephen, G. M., & McCabe, A. M. (1999). Landform modification by palaeo-ice streams in east-central Ireland. Annals of Glaciology, 28, 161-167.

Lewington, E. L., Livingstone, S. J., Clark, C. D., Sole, A. J., & Storrar, R. D. (2020). A model for interaction between conduits and surrounding hydraulically connected distributed drainage based on geomorphological evidence from Keewatin, Canada. The Cryosphere, 14(9), 2949-2976.

Lewington, E.L.M. (2020). New Insights into Subglacial Meltwater Drainage Pathways from the ArcticDEM. Ph.D. University of Sheffield, Sheffield.

Lundqvist, J. (1969). Problems of the so-called Rogen moraine. Sveriges geologiska undersökning, c648, 1–32.

LUNDQVIST, J. (1970). Studies of drumlin tracks in Central Sweden. Acta Geographia Lodziensia, vol. 24, p. 317-326..

Lundqvist, J. (1981). Moraine morphology: terminological remarks and regional aspects. Geografiska Annaler: Series A, Physical Geography, 63(3-4), 127-138.

Lundqvist, J. (1989). Rogen (ribbed) moraine—identification and possible origin. Sedimentary Geology, 62(2-4), 281-292.

Maclachlan, J. C., & Eyles, C. H. (2013). Quantitative geomorphological analysis of drumlins in the Peterborough drumlin field, Ontario, Canada. Geografiska Annaler: Series A, Physical Geography, 95(2), 125-144.

Markgren, M., & Lassila, M. (1980). Problems of moraine morphology: Rogen moraine and Blattnick moraine. Boreas, 9(4), 271-274.

McConnell, B., & Gatley, S. (2006). Bedrock geological map of Ireland, 1:500,000 scale. Geological Survey of Ireland, Dublin.

McKenzie, M. A., Simkins, L. M., Principato, S. M., & Munevar Garcia, S. (2022). Streamlined subglacial bedform sensitivity to bed characteristics across the deglaciated Northern Hemisphere. Earth Surface Processes and Landforms. 47 (9), 2341–2356.

Menzies, J. (1979). A review of the literature on the formation and location of drumlins. Earth-Science Reviews, 14(4), 315-359.

Mills, H.H. (1987). Morphometry of drumlins in the northeastern and north-central USA. In: Menzies, J., Rose, J. (Eds.), Drumlin Symposium. Balkema, Rotterdam, pp. 131–148.

Mitchell, W. A. & Riley, J. M. 2006: Drumlin map of the Western Pennines and southern Vale of Eden, Northern England, UK. Journal of Maps 2, 10-16.

Möller, P., & Dowling, T. P. (2015). The importance of thermal boundary transitions on glacial geomorphology; mapping of ribbed/hummocky moraine and streamlined terrain from LiDAR, over Småland, South Sweden. Gff, 137(4), 252-283.

Moellering, H. and Rayner, J. N. (1979) Measurement of Shape in Geography and Cartography . Report of the Numerical Cartography Laboratory, Ohio State University, NSF Grant No. SOC77-11318.

Napieralski, J., & Nalepa, N. (2010). The application of control charts to determine the effect of grid cell size on landform morphometry. Computers & geosciences, 36(2), 222-230.

Ng, F. S., & Hughes, A. L. (2019). Reconstructing ice-flow fields from streamlined subglacial bedforms: A kriging approach. Earth Surface Processes and Landforms, 44(4), 861-876.

Ó Cofaigh, C., Pudsey, C. J., Dowdeswell, J. A., & Morris, P. (2002). Evolution of subglacial bedforms along a paleo-ice stream, Antarctic Peninsula continental shelf. Geophysical Research Letters, 29(8), 41-1.

Porter C. et al. (2018). ArcticDEM, Version 3. https://doi.org/10.7910/DVN/OHHUKH.

Rose, J., & Letzer, J. M. (1975). Drumlin measurements: a test of the reliability of data derived from 1:25,000 scale topographic maps. Geological Magazine, 112, 361-371.

Rose, J., & Letzer, J. M. (1977). Superimposed drumlins. J. Glaciol. 18, 471-480.

Rose, J. (1987). "Drumlins as part of a glacier bedform continuum". In Drumlin Symposium, Edited by: Menzies, J. and Rose, J. 103–116. Rotterdam: A.A. Balkema.

Schumm, S. A. (1963). Sinuosity of alluvial rivers on the Great Plains. Geological Society of America Bulletin, 74(9), 1089-1100.

Sergienko, O. V., & Hindmarsh, R. C. (2013). Regular patterns in frictional resistance of ice-stream beds seen by surface data inversion. Science, 342(6162), 1086-1089.

Shaw, J. (1979). Genesis of the Sveg tills and Rogen moraines of central Sweden: a model of basal melt out. Boreas, 8(4), 409-426.

Shaw, J. (1983). Drumlin formation related to inverted melt-water erosional marks. Journal of Glaciology, 29(103), 461-479.

Shaw, J., Faragini, D. M., Kvill, D. R., & Rains, R. B. (2000). The Athabasca fluting field, Alberta, Canada: implications for the formation of large-scale fluting (erosional lineations). Quaternary Science Reviews, 19(10), 959-980.

Shaw, J., 2002. The meltwater hypothesis for subglacial bedforms. Quaternary International 90 (1), 5–22.

Shilts, W. W., Cunningham, C. M., & Kaszycki, C. A. (1979). Keewatin Ice Sheet—Re-evaluation of the traditional concept of the Laurentide Ice Sheet. Geology, 7(11), 537-541.

Shilts, W. W., Aylsworth, J. M., Kaszycki, C. A., & Klassen, R. A. (1987). Canadian shield. In Geomorphic Systems of North America (Vol. 2, pp. 119-161). Geological Society of America Boulder, Colorado.

Smalley, I., & Warburton, J. (1994). The shape of drumlins, their distribution in drumlin fields, and the nature of the sub-ice shaping forces. Sedimentary geology, 91(1-4), 241-252.

Smith, M. J., & Wise, S. M. (2007). Problems of bias in mapping linear landforms from satellite imagery. International Journal of Applied Earth Observation and Geoinformation, 9(1), 65-78.

Spagnolo, M., Bartholomaus, T. C., Clark, C. D., Stokes, C. R., Atkinson, N., Dowdeswell, J. A., ... & Pritchard, H. D. (2017). The periodic topography of ice stream beds: Insights from the Fourier spectra of mega-scale glacial lineations. Journal of geophysical research: earth surface, 122(7), 1355-1373.

Sookhan, S., Eyles, N., Bukhari, S., & Paulen, R. C. (2021). LiDAR-based quantitative assessment of drumlin to mega-scale glacial lineation continuums and flow of the paleo Seneca-Cayuga paleo-ice stream. Quaternary Science Reviews, 263, 107003.

Sookhan, S., Eyles, N., & Bukhari, S. (2022). Drumlins and mega-scale glacial lineations as a continuum of subglacial shear marks: A LiDAR based morphometric study of streamlined surfaces on the bed of a Canadian paleo-ice stream. Quaternary Science Reviews, 292, 107679.

Stokes, C. R., & Clark, C. D. (1999). Geomorphological criteria for identifying Pleistocene ice streams. Annals of glaciology, 28, 67-74.

Stokes, C. R., & Clark, C. D. (2002). Are long subglacial bedforms indicative of fast ice flow?. Boreas, 31(3), 239-249.

Stokes, C. R., Clark, C. D., & Winsborrow, M. C. M. (2006a). Subglacial bedform evidence for a major palaeo-ice stream and its retreat phases in Amundsen Gulf, Canadian Arctic Archipelago. Journal of Quaternary Science: Published for the Quaternary Research Association, 21(4), 399-412.

Stokes, C. R., Clark, C. D., Lian, O. B., Tulaczyk, S. (2006b). Geomorphological map of ribbed moraines on the Dubawnt Lake Palaeo-Ice stream bed: a signature of ice stream shut-down? Journal of Maps 2 (1), 1–9.

Stokes, C. R., Clark, C. D., Lian, O. B., Tulaczyk, S. (2007). Ice stream sticky spots: a review of their identification and influence beneath contemporary and palaeo-ice streams. Earth-Science Reviews 81 (3–4), 217–249.

Stokes, C. R., Lian, O. B., Tulaczyk, S., & Clark, C. D. (2008). Superimposition of ribbed moraines on a palaeo-ice-stream bed: implications for ice stream dynamics and shutdown. Earth Surface Processes and Landforms: The Journal of the British Geomorphological Research Group, 33(4), 593-609.

Stokes, C. R., Spagnolo, M., Clark, C. D., Cofaigh, C. Ó., Lian, O. B., & Dunstone, R. B. (2013). Formation of mega-scale glacial lineations on the Dubawnt Lake Ice Stream bed: 1. size, shape and spacing from a large remote sensing dataset. Quaternary Science Reviews, 77, 190-209.

Stokes, C. R., Margold, M., & Creyts, T. T. (2016). Ribbed bedforms on palaeo-ice stream beds resemble regular patterns of basal shear stress ('traction ribs') inferred from modern ice streams. Journal of Glaciology, 62(234), 696-713.

Storrar, R. D., Stokes, C. R., & Evans, D. J. (2013). A map of large Canadian eskers from Landsat satellite imagery. Journal of maps, 9(3), 456-473.

Synge, F. M., & Stephens, N. (1960). The Quaternary period in Ireland—an assessment, 1960. Irish Geography, 4(2), 121-130.

Van Landeghem, K. J., & Chiverrell, R. C. (2020). Bed erosion during fast ice streaming regulated the retreat dynamics of the Irish Sea Ice Stream. Quaternary Science Reviews, 245, 106526.

Vérité, J., Ravier, É., Bourgeois, O., Pochat, S., Lelandais, T., Mourgues, R., ... & Atkinson, N. (2021). Formation of ribbed bedforms below shear margins and lobes of palaeo-ice streams. The Cryosphere, 15(6), 2889-2916.

Vérité, J., Ravier, É., Bourgeois, O., Bessin, P., Livingstone, S. J., Clark, C. D., ... & Mourgues, R. (2022). Formation of murtoos by repeated flooding of ribbed bedforms along subglacial meltwater corridors. Geomorphology, 408, 108248.

Wagner, K. G (2014). Ribbed moraines and subglacial geomorphological signatures of interior-sector palaeo-ice sheet dynamics. Unpublished MSc Brock University, Canada, 274 pp.

Wellner, J. S., Lowe, A. L., Shipp, S. S., & Anderson, J. B. (2001). Distribution of glacial geomorphic features on the Antarctic continental shelf and correlation with substrate: implications for ice behavior. Journal of Glaciology, 47(158), 397-411.

Winsborrow, M., Clark, C., & Stokes, C. (2004). Ice streams of the Laurentide ice sheet. Géographie physique et Quaternaire, 58(2-3), 269-280.

Zheng, W., Pritchard, M. E., Willis, M. J., & Stearns, L. A. (2019). The possible transition from glacial surge to ice stream on Vavilov Ice Cap. Geophysical Research Letters, 46(23), 13892-13902.

Zoet, L. K., Rawling III, J. E., Woodard, J. B., Barrette, N., & Mickelson, D. M. (2021). Factors that contribute to the elongation of drumlins beneath the Green Bay Lobe, Laurentide Ice Sheet. Earth Surface Processes and Landforms, 46(13), 2540-2550.